

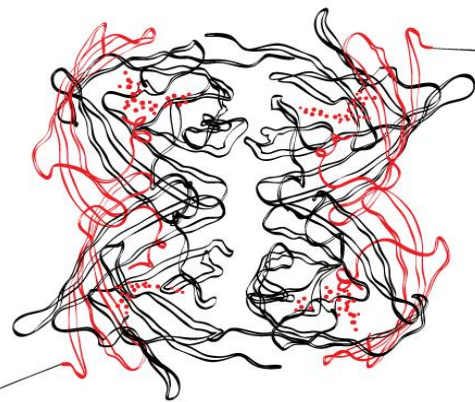
IMPACT MECHANICS OF HELMET COMPONENTS

Internship (course code: 191199154)



Bennie van den Hazel

14 January 2015



Internship Report

Impact Mechanics of Helmet Components

Submitted by:

Bennie van den Hazel

Student number: s1010182 (UT)
Staff number: e18354 (RMIT)
Email: b.vandenhazel@student.utwente.nl

Number of pages: 31
Number of appendices: 3
Date of publication: 14 January 2015
Period: August 25th 2014 – December 5th 2014
European Credits: 20

RMIT University
School of Aerospace, Mechanical and Manufacturing
Engineering

Bundoora East Campus, VIC 3083
Melbourne
Australia

Supervisor:
Prof. Dr. Franz Konstantin Fuss
franz.fuss@rmit.edu.au

University of Twente
Faculty of Engineering Technology
Chair of Applied Mechanics

Drienerlolaan 5, 7522 NB
Enschede
The Netherlands

Supervisor:
Prof. Dr. ir. André de Boer
a.deboer@ctw.utwente.nl

Summary

In horse riding head protection of the jockey is important, therefore this research is performed in collaboration with Albion. Albion is specialized in many sports protection gear. The aim of this research is to test, model and optimize impact absorbing material to develop a selection guide and a complete set of data that describes the performances and properties of different liners for jockey helmets. Further the padding should facilitate a good fit, thermal comfort and be lightweight.

In general, solid polymeric foams can be divided into closed-cell and open-cell foams. Closed-cell foams consist of closed cells which are full of gas. Open-cell foams are softer and air fills all of the spaces in the material. Three phases of deformation are commonly observed during compression of polymeric foams, namely quasi-static linear response, collapse plateau and densification region. An important independent parameter in designing an impact layer is the shoulder point, which is defined as the optimal ratio W/σ , where W is energy density [J/m^3] and σ is stress [MPa]. At this point the stress-strain curve switches from collapse plateau to densification region. The most efficient foam is the one that absorbs the most energy up to the lowest possible maximum stress during deformation, thus the one with the highest shoulder point. Foams exhibit strain rate dependency as they are made of visco-elastic materials. The faster the strain rate, the stiffer the material. Therefore two load cases are observed, quasi-static and dynamic compression. Strain rates up to 1000 s^{-1} show quasi-static response.

Various materials are tested to find the optimal material for impact absorbing. This includes 24 different foams and 21 different structures. All uniaxial quasi-static compression experiments are done with an **INSTRON** 5569 Material Testing Machine, using a 50 kN load cell at a maximum speed of 500 mm/min. All uniaxial dynamic compression experiments are performed with a striker drop test with a drop mass of 5.04 kg from a maximum height of 3 meter. The acceleration is measured by a **KISTLER** 8715A acceleration sensor. In addition to this sensor, a piezoresistive sensor is designed, made and used.

From the quasi-static compression can be concluded that cardboard has the best performances. All investigated materials show strain rate dependency, which means that they can absorb more energy at higher strain rates. Combined performance of an impact layer in combination with a soft comfort layer is always worse, because equivalent stiffness is less than both separate stiffness's. On top of this padding a thin soft layer can be used to increase the comfort for the jockey, but this is out of the scope of this research. Quasi-static results give a good insight in the impact absorbing characteristics of all materials. In addition, simulations of higher impact energies from quasi-static compression data showed expected characteristics.

In case of dynamic compression experiments lower shoulder points are found, as a result of high peak moduli. Moreover, acceleration data extracted from the impact tester could not be integrated twice to get the travel distance. To avoid double integration the impact energy density is divided by the peak stress to investigate impact characteristics of each material. From many experiments can be concluded that D30 Aero never reach densification, because of shear thickening. Other experiments show the linear elastic, collapse plateau and densification. It can be concluded that more dynamic compression experiments and research has to be done to finalize and optimize the design guide for jockey helmets.

Sensor less sensing (SLS) did not work properly and it is unclear whether it measures the right peak acceleration or not. SLS is not optimized in this research, because it is in addition to the acceleration sensor of the impact tester. The safety of jockeys has high priority, so therefore the padding must be designed on HIC less than 1000 and acceleration of a human head less than 300g, where g is the standard gravity constant. The design guide is based on quasi-static results to select and design jockey helmets. It shows the six best solutions sorted on increasing density to design lightweight, where the required layer thickness is less than the allowable layer thickness.

Preface and Acknowledgements

This report shows the results and findings of my internship at the Royal Melbourne Institute of Technology (RMIT) University at the School of Aerospace, Mechanical and Manufacturing Engineering from August to December 2014. The internship is an integral part of the Master in Mechanical Engineering at the University of Twente.

My internship covers diagnostics, testing, modelling, establishment of a database, optimization and development of a selection guide for helmet paddings. The collaboration partner, Albion, has only limited research and testing facilities at their disposal of test methods, therefore I did this research at RMIT University.

A version of *Foam Mechanics: Evaluating Performance Based On Energy Absorption At Optimal Strain* has been published during the 1st International Conference in Sports Science & Technology in Singapore on 11-12 Dec 2014. I have worked and continued on this research, together with Aaron Belbasis, the main author of the paper; therefore I am co-author of this paper.

Further two more papers will be published in the near future. One will be about the relation between quasi-static and dynamic compression shoulder points and a second paper will discuss foam behaviour at various impact energies. I will be co-author of these papers as well, because I have performed most experiments and analyses, including interpretation of the results.

This research could not have been done without the invaluable help of Prof. Franz ‘Tino’ Fuss during this internship. He often had additional research topics, which made this internship challenging and educational for me. A second thanks has to go to Aaron Belbasis for his company and guidance during the whole period, without him it would have been less fun and educational than it was now. Thanks for Yehuda Weizman for his company as well. Of course my fiancée Pauline and my family deserve a thank you, because they supported me through the whole process of arranging everything and actually departing for a period of four months. Above all, I would like to thank God for giving me the opportunity, power and endurance to complete this internship.

Melbourne, December 2014
Bennie van den Hazel

Index

Summary.....	II
Preface and Acknowledgements.....	III
Index.....	IV
1. Introduction.....	1
1.1 Research Aim.....	1
1.2 Company Background.....	1
1.3 Structure of report	1
2. Literature Review.....	2
2.1 General foams.....	2
2.2 Existing models.....	3
2.3 Strain rate dependency	4
2.4 Visco-elastic modelling.....	5
2.5 Shoulder Point.....	5
2.6 Mechanics of Materials	6
2.6.1 Open-cell.....	6
2.6.2 Closed-cell.....	6
2.7 Head Injury Criterion	7
2.8 Piezoresistive sensing.....	7
2.9 Thermal properties.....	7
3. Method.....	8
3.1 Materials.....	8
3.2 Testing procedure	9
3.2.1 Quasi-static compression.....	9
3.2.2 Dynamic compression.....	10
4. Analysis.....	13
4.1 Quasi-static compression	13
4.1.1 General analysis.....	13
4.1.2 Viscosity.....	14
4.2 Simulation.....	14
4.3 Dynamic compression	15
4.3.1 General analysis.....	15
4.3.2 Sensor less sensing.....	16
4.4 Selection of foams.....	17
4.4.1 Main criteria	17
4.4.2 Breathability & Repeatability.....	17
5. Results.....	18
5.1 Quasi-static compression	18

5.1.1	General results	18
5.1.2	Combined performance.....	20
5.1.3	Viscosity.....	21
5.1.4	Shoulder points.....	22
5.1.5	Case study company results	22
5.2	Simulation.....	24
5.3	Dynamic compression	24
5.3.1	Impact tester	24
5.3.2	Sensor less sensing.....	27
5.4	Design guide.....	28
6.	Conclusions and Discussion	30
6.1	Conclusions	30
6.2	Discussion.....	30
7.	Recommendations	31
8.	Bibliography	32
	Appendix A – Derivation open-cell	1
	Appendix B – Derivation closed-cell	3
	Appendix C – Codes.....	4

1. Introduction

This chapter discusses the research aim, company background and structure of the report.

1.1 Research Aim

Although the primary role of a helmet liner is to attenuate impact, the liner should also facilitate a good fit, thermal comfort and be lightweight. Therefore this research contains the full property and performance characterizations of the current jockey helmet liners and the next generation of liners or padding systems identified as suitable solutions.

Important outcomes are a complete set of data that describes the performance and properties of different liners. Further an expert system in any form that identifies a liner system based on a limited set of input data. The expert system will serve as a decision guide for selecting the optimal liner for specific impact scenarios. The liner system will be recommended by its type, geometry and properties.

So in short, the purpose of this research is to test, model and optimize impact absorbing material to develop a selection guide for jockey helmet paddings.

1.2 Company Background

Albion, which began in 1941, has kept its factory in Sydney after moving its headquarters to Melbourne a few years ago and are now an industry innovator through the development of sports protective gear. Albion was the first company to make cricket helmets and became through this leaders in cricket head protection and manufacturers of the world's first cricket helmet at the time of the World Series Cricket in 1977.

Since the 1970's the need for athletes to reach a personal best became more apparent and Albion's competitive desire ensured it was part of the winning formula. Now they are specialized in many sports protection gear, including cricket head protection, traditional sporting headwear and horse riding head protection. Albion's full attention is on the voice of the athlete, so their next stage of head protection will include the technology of 3D printing. A jockey helmet of Albion can be seen in Figure 1 [1].



Figure 1 Jockey helmet

1.3 Structure of report

This report describes all aspects of the research, which aim is described in section 1.1. In the next chapter literature about foams is reviewed. Hereafter the test method is described, including identification of the materials and test procedure. This is followed by the way of analysing data from experiments and the results in chapters 4 and 5, respectively. In chapter 6 conclusions are summarized and subsequently some discussion points are mentioned. Hereafter recommendations for the company and further research opportunities are given and these are followed by a bibliography. Finally after the main part of the report appendices can be found.

2. Literature Review

In this chapter literature about foams is discussed. First some general information about foams and hereafter information about existing models for the stress-strain curve, strain rate dependency, visco-elastic modelling, the definition of the shoulder point, a derivation of the optimal strain, which is the strain at the shoulder point, for open- and closed-cell foams and the final topics mentioned in this chapter are the Head Injury Criterion, piezoresistive sensing and thermal properties. All these topics form a basis for the rest of this research.

2.1 General foams

A foam is a substance that is formed by trapping pockets of gas in a liquid or solid. Foams are often used because of their ability to absorb energy and are lightweight in comparison with other materials [2]. Foams are anisotropic materials, which means that their properties are independent of the direction of the impact.

An important division of solid polymeric foams is into closed-cell and open-cells foams [3][4][5]. Closed-cell foams consist of closed cells which are full of a special gas or air. Closed-cell foams have varying degrees of hardness, depending on their densities. When a closed-cell foam is compressed, energy is absorbed in the bending, buckling and stretching of the cell walls and in the compression of the gas contained within the cells. The advantage of closed-cell foam is its strength, higher insulation factor and greater resistance to the leakage of air or water vapour. For jockey helmets the higher insulation factor is a disadvantage, because of thermal comfort.

Open-cell foams are soft, because the cell walls are broken and air fills all of the spaces in the material. Normally the density of open-cell foams is low compared to closed-cells foams. When an open-cell foam is compressed, energy is mainly absorbed in the bending and buckling of the cell walls. The advantage of open-cell foam is the low density and because of that less material usage, which results in less expensive and lightweight material. Every foam between open- and closed-cell foams is called reticulated foam.

Three phases of deformation are commonly observed during compression of polymeric foams. The first phase is quasi-static linear response, where stress increases linearly with deformation and the strain is recoverable. In this phase elastic deformation of the cell walls and first buckling occur. The second phase is characterized by continued deformation at relatively constant stress, known as the stress or collapse plateau and provides the bulk of the energy absorption capabilities for the foam. In this phase the mechanism of buckling and collapse become more pronounced, which is manifested in large strains at almost constant stress. The level of plateau depends on the material, density and strain rate. The final phase of deformation is densification where the foam begins to respond as a compacted solid. At this point the cellular structure within the material is collapsed and further deformation requires compression of the solid foam material. The mechanism of cell deformation and collapse depends on the relative density of the cellular structure. While the cell walls are subjected to buckling and bending at relative low densities, they shear at relative higher densities since the cell walls are too short or too thick to bend [6].

A typical foam stress-strain curve is shown below in Figure 2. Elastic, plastic and brittle foams have these three-part stress-strain curves under quasi-static compression. Difference in energy put into the foam and released from the foam is called hysteresis and this energy dissipates as heat. The hysteresis is the area between the upper and lower line in Figure 2.

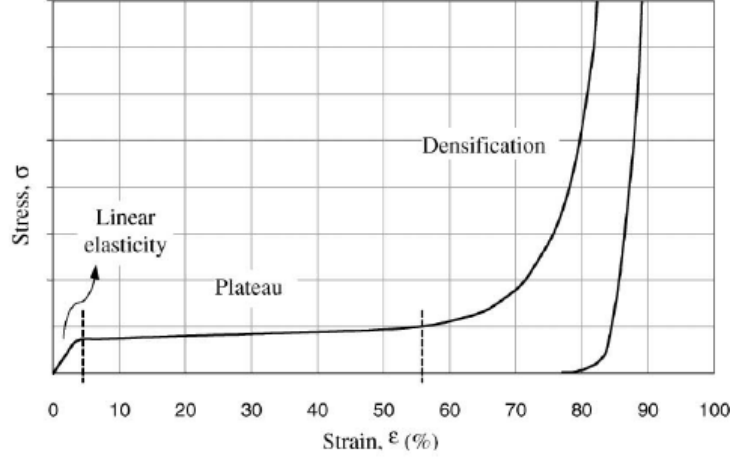


Figure 2 Typical stress-strain curve of foam [5][7]

Besides foams a lot of other cell structures are used to attenuate impact. Therefore in this research some other provided structures are investigated, as shown in Figure 7 and Figure 8. These structures are not classified as foams, but they consist of plastic or rubber-like material, which absorbs the energy during an impact.

2.2 Existing models

The properties and performances of foams can be described by different models [8]. In general there are two models, phenomenological models and micro-mechanical models. Phenomenological models give the best fit of the experimental mechanical behaviour and the micro-mechanical models are based on the analysis of the deformation mechanisms of the micro-cell structure under loading. First the Gibson model [5] is discussed and subsequently the Rusch model [9].

The Gibson model is a micro-mechanical model and divides the compression stress-strain curve into three regions. The linear elastic region is described by equation (1), plateau region by equation (2) and densification region by equation (3), where σ and ϵ are engineering stress and engineering strain, respectively, considered positive in compression. As shown the Gibson model needs five parameters, where D and m are density independent.

$$\sigma = E\epsilon \quad \text{if } \sigma \leq \sigma_{\text{yield}} \quad (1)$$

$$\sigma = \sigma_{\text{yield}} \quad \text{if } \epsilon_{\text{yield}} \leq \epsilon \leq \epsilon_D \left(1 - D^{-\frac{1}{m}}\right) \quad (2)$$

$$\sigma = \sigma_{\text{yield}} \frac{1}{D} \left(\frac{\epsilon_D}{\epsilon_D - \epsilon}\right)^m \quad \text{if } \epsilon > \epsilon_D \left(1 - D^{-\frac{1}{m}}\right) \quad (3)$$

The Rusch model is a phenomenological model and the sum of two power laws, as can be seen in equation (4).

$$\sigma = A\epsilon^m + B\epsilon^n \quad \text{with } 0 < m < 1, 1 < n < \infty \quad (4)$$

Here again σ and ϵ are engineering stress and engineering strain, respectively, considered positive in compression. This model needs four parameters to describe the stress-strain curve, but a drawback is the inaccuracy in describing the densification region.

Many other models can be found in literature, but only the two models mentioned above are further investigated in this report given the dominant literature behind the above methods.

2.3 Strain rate dependency

Strain rate dependency is an inherent characteristic of visco-elastic materials, the faster the strain rate, the stiffer the material. In impact testing two load cases are observed, namely quasi-static and dynamic compression. Quasi-static compression means the load is applied at a relatively slow strain rate and therefore the inertia force is very small and can be ignored. Quasi-static compression is time independent. In general, all foams show a quasi-static response up to strain rates of 1000 s^{-1} , which is an important consideration that data should not be extrapolated from lower strain rates [10].

On the other hand, dynamic compression results in vibration of the structure and is time dependent. Foams react different on quasi-static and dynamic compression, which is called the strain rate dependency. The cellular material is able to absorb energy through its deformation during the loading process. For foams yield the higher the strain rate, the higher the capability of energy absorption through deformation, as can be seen below in Figure 3.

Very fast deformation at high strain rates results in temperature change of the base material, which affects its mechanical properties. For impact loading the loading time might be short enough to justify neglecting the temperature effect by heat conduction in the base material [11].

Open-cell foams are more strain rate dependent than closed-cell foams. The fluid flow is strongly influenced by the compression rate. When a foam deforms, the air is compressed or forced outside, depending on the foam cellular structure (closed-cells or open-cells). For foams the stress-strain curves for increasing strain rate can be seen below in Figure 3. As shown with increasing strain rate an increased elastic modulus, increased plateau region and a decreased densification strain is observed.

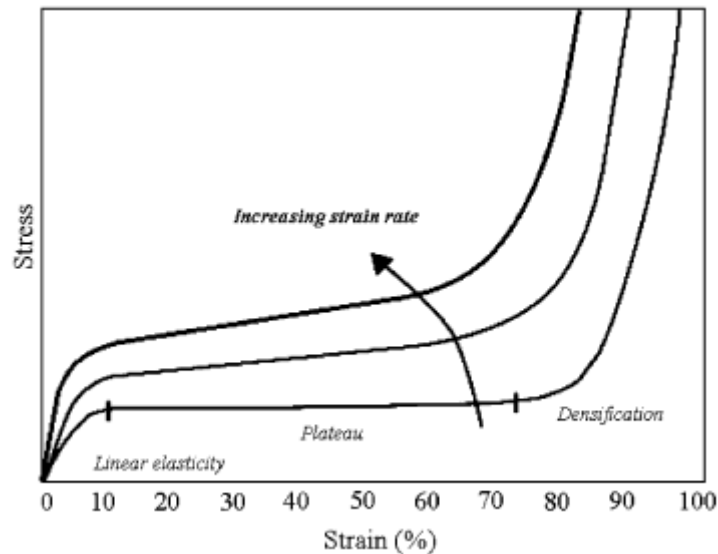


Figure 3 Influence increasing strain rate [10]

The strain rate sensitivity is assumed by equation (5), motivated by the work of Nagy [12], where $\sigma_0(\epsilon)$ represents the nominal stress response at a constant quasi-static strain rate $\dot{\epsilon}_0$ and $n(\epsilon) = a + b\epsilon$ is the power coefficient for rate dependency, where a and b are material constants.

$$\sigma(\epsilon) = \sigma_0(\epsilon) \left(\frac{\dot{\epsilon}}{\dot{\epsilon}_0} \right)^{n(\epsilon)} \quad (5)$$

The strain rate dependency of the mechanical behaviour of foams can be related to the visco-elastic properties, and therefore the modelling of visco-elastic behaviour is described in section 2.4.

2.4 Visco-elastic modelling

A simple linear visco-elastic model requires three parts, two springs and one damper. All foams are visco-elastic to some extent. The foams show hysteresis on unloading. Visco-elastic response, where the compression stress σ is proportional to the compression strain rate $d\varepsilon/dt$ and the viscosity parameter η yields as equation (6) [13].

$$\sigma = \eta \frac{d\varepsilon}{dt} \quad (6)$$

The Voigt mechanical model, using a spring and dashpot in parallel, is often used to describe creep. Equation (7) shows the relation between the total force F and the deflection x , where k is the spring stiffness and n the damper constant.

$$F = kx + n \frac{dx}{dt} \quad (7)$$

Then the constitutive equation for linear visco-elastic material becomes as equation (8).

$$\sigma = E\varepsilon + \eta \frac{d\varepsilon}{dt} \quad (8)$$

Nonlinearity can be attributed to this linear model to describe the foam behaviour in more detail, because the material properties of foams change if the strain rate is increased. For example, the compressive yield stress of rigid foams tends to increase linearly with the logarithm of the strain rate [10]. In general nonlinear models require more parameters. Using the nonlinear power law model as shown below in equation (9) [14], it is possible to compute the viscosity parameter η and the strain rate independent elasticity parameter R .

$$\ln(E) = \eta \ln\left(\frac{\dot{\varepsilon}_{\text{mean}}}{\varepsilon}\right) + \ln(R) \quad (9)$$

This model is only valid if, and only if, R and η are constants and do not change with strain. The Young's modulus is inherent dependent on the strain rate. Plotting $\ln(E)$ against $\ln\left(\frac{\dot{\varepsilon}_{\text{mean}}}{\varepsilon}\right)$ the intercept and gradient of the linear regression are R and η , respectively. The viscosity parameter gives important information about the sensitivity of strain rate dependency and is a measure of its resistance to deformations.

2.5 Shoulder Point

An optimum energy-absorbing material needs to dissipate the kinetic energy of the impact while keeping the acceleration (or jerk) of it below some limit, thus, resulting in safe acceleration of a human head. This means the most efficient foam is the one that absorbs the most energy up to the lowest possible maximum stress during deformation, so the one with the highest ratio W/σ . This point is known as shoulder point or cushion factor [5]. Figure 4 shows this shoulder point in relation with the stress-strain curve and energy curve. At the shoulder point the stress-strain curve switches from collapse plateau to densification region. This shoulder point is an important design parameter for foams. It is worth to remark that an ideal foam is not the one with the highest shoulder point, but it is the one with a plateau stress just below the allowable stress. This means an energy density which is equal to the kinetic energy to be absorbed per unit volume of the material.

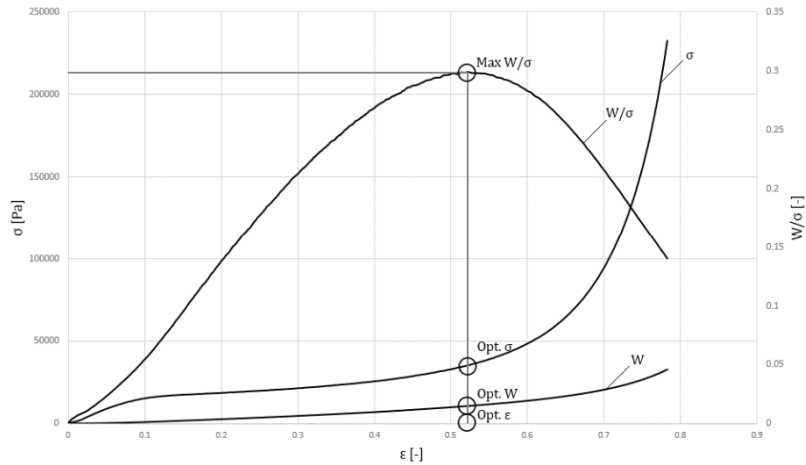


Figure 4 Relation between shoulder point and optimal stress, strain and energy density

In case of closed-cell foams shoulder points at various densities are expected to be on a curved envelope [5]. This phenomena occurs, because at high densities the cell-wall deformation is the dominant energy-absorbing process, while at low densities compression of the gas in the cell becomes dominant. For open-cell foams yield that the cell-wall deformation is the dominant energy-absorbing process, so the shoulder points at various densities are expected on a straight envelope.

2.6 Mechanics of Materials

In this section models of the open-cell and closed-cell foams are made to predict the optimal strain, which is the strain at the shoulder point.

2.6.1 Open-cell

For open-cell foams only buckling of the cell wall is assumed, which means the effects of air flow are neglected. The structure of open-cell foams is modelled like buckling of a slender rod and it is assumed that buckling starts in the middle of this rod. The derivation for open-cell foams can be found in appendix A, where a distinction is made between pinned-pinned and fixed-fixed support. It was determined that the optimal strain at shoulder point is 50% for pinned-pinned support and 25% for fixed-fixed support.

2.6.2 Closed-cell

For closed-cell foams a different model is needed, because of the compression of the enclosed gas. This calculation uses the model defined by Rusch [9], as shown in Figure 5.

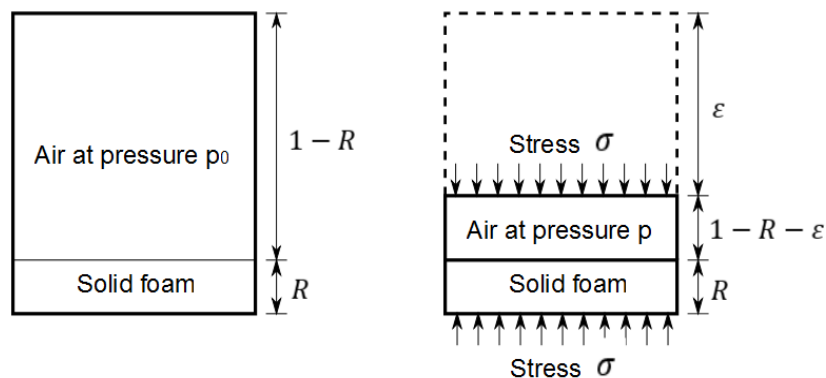


Figure 5 Model closed-cell foam

Assumed that there is no lateral expansion, which means the Poisson ratio is zero, the volumetric strain is equal to the compressive strain, isothermal gas compression and incompressible foam

walls. The derivation can be found in appendix B and it was determined that the optimal strain at shoulder point for closed-cell foams is 68.38%.

2.7 Head Injury Criterion

The Head Injury Criterion (HIC) is a measure of the likelihood of head injury arising from an impact [17]. The HIC includes the effects of head acceleration and the duration of the acceleration, as can be seen in equation (10), where t_1 and t_2 are the initial and final times of the interval during which HIC attains a maximum value and $a(t)$ is the acceleration measured in g (standard gravity acceleration).

$$\text{HIC} = \left\{ \left[\frac{1}{t_2 - t_1} \int_{t_1}^{t_2} a(t) dt \right]^{2.5} (t_2 - t_1) \right\}_{\max} \quad (10)$$

As a rule of thumb, it is highly recommended that $\text{HIC} < 1000$ and $a_{\max} < 300g$ [18], so this is set as the desired peak deceleration.

2.8 Piezoresistive sensing

In this research a piezoresistive sensor is used during the impact experiments. The resistance change (piezoresistive effect) is a change in electrical resistivity of the conductive material when mechanical strain is applied. The resistance value of a resistor $[\Omega]$ with a conductor length l [m] and cross-sectional area of the current flow A [m²] is given by equation (11), where ρ is the bulk resistivity [Ωm].

$$R = \rho \frac{l}{A} \quad (11)$$

The resistance value is determined by the dimensions and the bulk resistivity. Firstly the cross-sectional area of the conductive compound may change in case of an impact, due to the Poisson's ratio of this compound. Secondly the resistance changes as a function of strain. The magnitude of resistance change from this last principle is much greater than the first one, therefore the changes of the cross-sectional area are neglected [19].

The change in resistance is linearly related to the applied strain and the amplification factor between strain and resistance change is called the Gauge Factor (G). An explicit expression for G , if $\sigma = \epsilon E$, can be seen below in equation (12) [20].

$$\frac{\Delta R}{R} = G \cdot \frac{\Delta L}{L} \rightarrow G = \frac{\Delta R}{\epsilon R} \quad (12)$$

Advantages of using a piezoresistive sensor are low costs, high sensitivity, excellent repeatability and can be cut to the optimal shape desired. On the other hand, resistance changes with a change in temperature and the conductive compound may shift during impact.

2.9 Thermal properties

Several factors influence the thermal properties of a foam. Firstly the volume fraction of the solid phase. The higher this fraction, the better the breathability. Secondly the cell size influences the breathability. Large cell size, which virtually increases convection and radiation through repeated absorption, leads to better breathability of the padding. Last property mentioned here is the conductivity of the enclosed gas, although closed-cell foams have definitely worse breathability [5].

3. Method

The purpose of this research is to optimize helmet padding for impact absorption. This is done by determining the shoulder point, at which optimal energy to stress ratio is achieved. In this chapter the method is discussed on the basis of material description and testing procedure. Last section discusses both quasi-static and dynamic compression.

3.1 Materials

Various materials are tested to find the optimal helmet padding. This includes 24 different foams and 21 different structures. Prior to testing the cellular structure of the 24 different foams are visually inspected by using a LEICA EZ4D microscope (35x magnification). Most results are shown below in Figure 6, however not all microscopic figures are in this report. The different structures are shown below in Figure 7 and Figure 8. It is worth to remark that most structures are not isotropic, which means that the properties are dependent on the direction of impact.

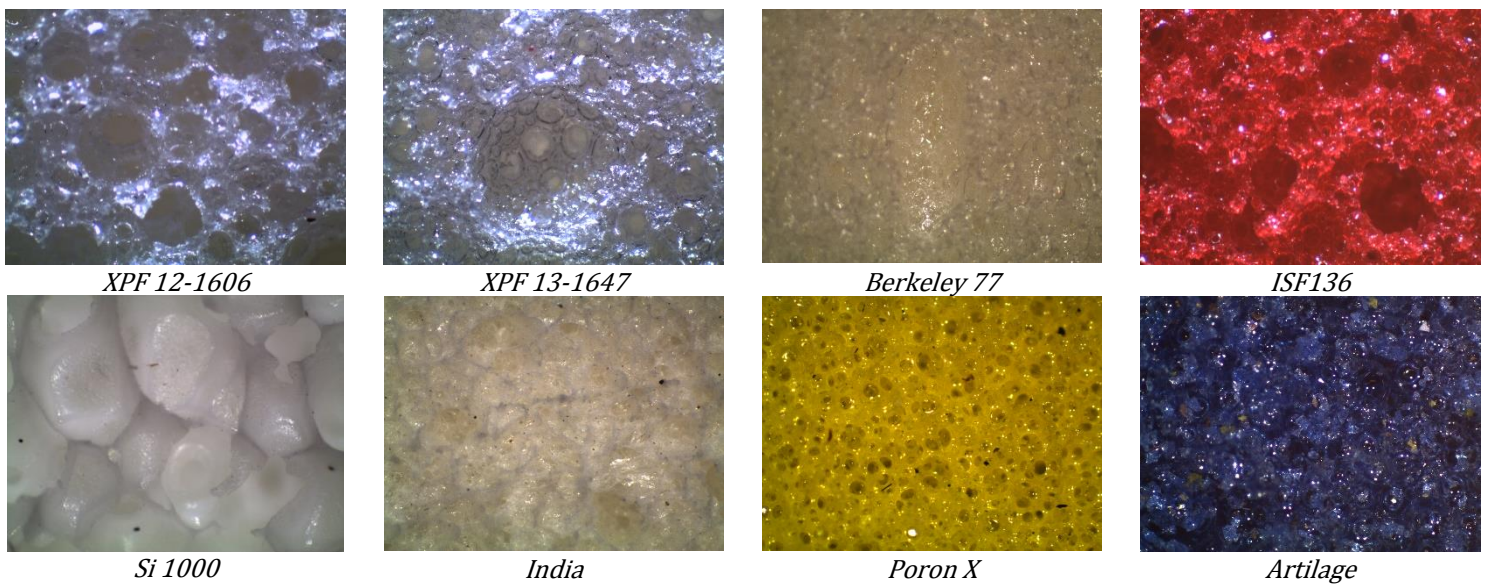


Figure 6 Results microscopic research

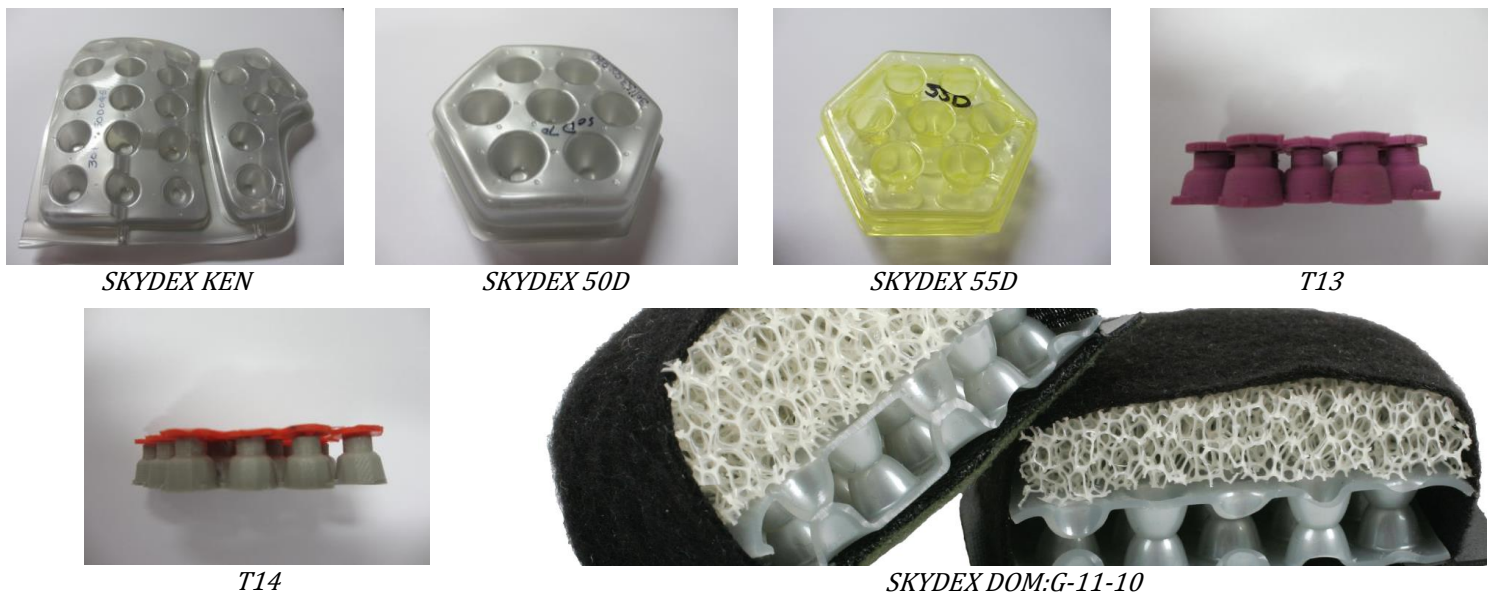


Figure 7 Different structures (first part)



Poron Shoulder



Poron Hip



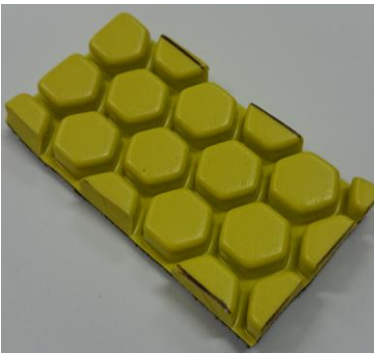
Poron B-Guard



EPS Black



EPS White



Poron X-pad



Skydex T26



Cardboard

Figure 8 Different structures (second part)

3.2 Testing procedure

First it is good to consider that compression testing is double-sided, although the real impact is single-sided. Furthermore the experiments are performed at constant room temperature. All materials are tested under quasi-static compression to determine their energy absorption characteristics and a selection of the materials are tested under dynamic compression to investigate impact behaviour.

3.2.1 Quasi-static compression

The uniaxial quasi-static compression experiments are done with an **INSTRON** 5569 Material Testing Machine, using a 50 kN load cell. The speed range of this machine is 0.005 – 500 mm/min and **BLUEHILL 2** software is needed for extracting data from the machine. Experiments are done at two constant strain rates by a ramp up/ramp down load profile. Due to the limitations of the testing equipment a limiting strain rate of 0.28 s^{-1} was calculated (see equation (17)) and the other strain rate was selected at two orders of magnitude slower (0.0028 s^{-1}). Prior to testing most materials are split into two samples, because each material is tested at two different strain rates. Then the dimensions and weights of all samples are determined to calculate the areas and densities. In general the samples are tested till $\epsilon_{\max} = 80\%$ to make sure the shoulder point is reached. The strain level is gained by setting the travel distance.

Due to various thicknesses of the samples, maximum crosshead speed for each sample is determined by scaling it to the thickest sample. The maximum speed of the **INSTRON** machine is 500 mm/min, so this speed is used at the thickest sample. A gap of 1 mm is added to ensure the

foam is unloaded at the start of the experiment. A schematic overview of the test setup can be seen below in Figure 9.

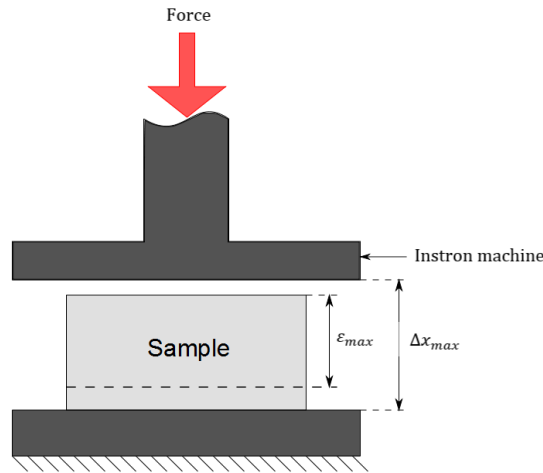


Figure 9 Test setup quasi-static compression

The following calculations are needed to determine the input parameters for the **INSTRON** machine. First the maximum travel distance Δx_{\max} [m] is calculated by equation (13), where ϵ_{\max} is the maximum applied strain and h_{\max} the maximum thickness [m].

$$\Delta x_{\max} = (\epsilon_{\max} \cdot h_{\max}) + 0.001 \quad (13)$$

Time t [sec] is calculated by equations (14) and (15).

$$\Delta t_{500} = \frac{\Delta x_{\max} \cdot 60 \cdot 1000}{500} \quad (14)$$

$$\Delta t_5 = \frac{\Delta x_{\max} \cdot 60 \cdot 1000}{5} \quad (15)$$

Crosshead speed v [mm/min] is calculated by equation (16), where Δx_{sample} is the travel distance determined by the sample thickness.

$$v = \frac{\Delta x_{\text{sample}} \cdot 60 \cdot 1000}{\Delta t_{\max}} \quad (16)$$

Then the strain rate $\dot{\epsilon}$ [s^{-1}] is defined as equation (17).

$$\dot{\epsilon} = \frac{v}{h \cdot 60 \cdot 1000} \quad (17)$$

Sample frequency f_{sample} [Hz] is calculated by equation (18), where f_{\max} is the maximum sample frequency. The sample frequency is adjusted to gain the same amount of data for each experiment. For high strain rates yield $f_{\max} = 500$ Hz and for low strain rates $f_{\max} = 5$ Hz.

$$f_{\text{sample}} = \frac{\Delta x_{\text{sample}} \cdot f_{\max}}{\Delta x_{\max}} \quad (18)$$

For analysing the quasi-static compression experiments time [sec], extension [mm] and load [N] are extracted from the **INSTRON** machine.

3.2.2 Dynamic compression

Strain rates up to 100 s^{-1} are common in impact applications, however these strain rates cannot be obtained with an universal testing machine. Therefore dynamic compression experiments are performed with a striker drop test. A schematic and real overview of the impact tester can be seen below in Figure 10.

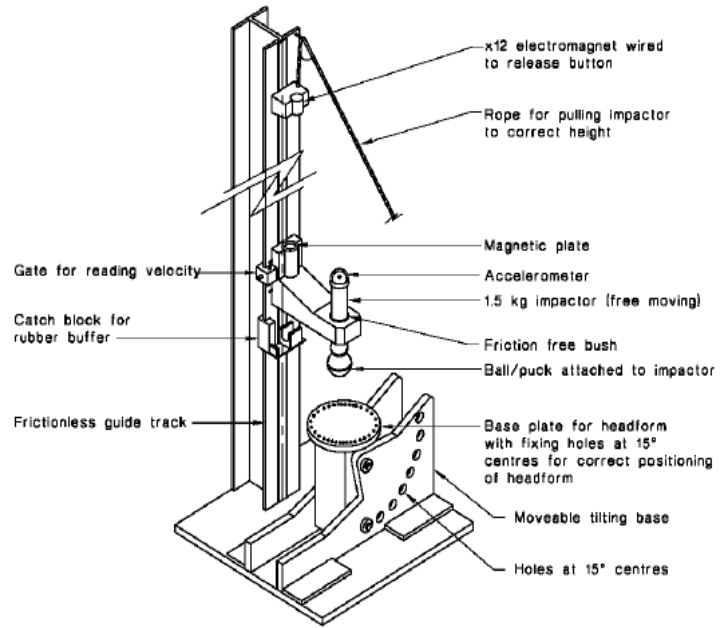


Figure 10 Impact tester

The impact tester drops a mass of 5.04 kg from a maximum drop height of 3 m. The acceleration is measured by a **KISTLER** 8715A acceleration sensor, which is mounted on the drop mass. This sensor is calibrated as 0.989 mV/g and a transverse sensitivity of 2.6%. It has an eigenfrequency of 70.0 kHz and the measuring range is ± 5000 g. The signal of this sensor is amplified by using a **KISTLER** amplifier (Type: 5134B). A low pass filter of 1 kHz is used and the time constant is 1 sec. The overload threshold is set to 100% and the current/bias is 4 mA/11.4 V. **CRICKETDAQ** is used for extracting data from the acceleration sensor with a sampling rate of 30 kHz, gain of 2 and scale of 1 mV/g. Previous experiments turned out that the acceleration data have to be multiplied by 500 if the gain is 2. The drop height [m] is adjusted to every sample by equation (19), to hit the sample over its optimal energy.

$$h = \frac{1.5 \cdot W_{\text{opt}} \cdot A \cdot t}{m_{\text{drop}} \cdot g} \quad (19)$$

In this equation W_{opt} is the optimal energy density [J/m^3], $A \cdot t$ is the volume of the sample [m^3], m_{drop} is the mass [kg], which is dropped onto the sample and g is the standard gravitation constant. There is 50% added to the optimal energy to make sure that the shoulder point is reached. The test sample and sensor less sensing (SLS) are positioned between a plastic top plate and the aluminium fixed world.

In addition to measuring acceleration, SLS is used during the impact experiments. Therefore a piezoresistive sensor is made, which mainly consists of a conductive compound and two aluminium electrodes. For this piezoresistive sensor Velostat is used as conductive compound, which is a polymeric foil impregnated with carbon black to make it electrically conductive. Velostat is fabricated by Minnesota Mining and Manufacturing Company (3M) and five layers of this compound are used for reasons of stability and to prevent shifting of the baseline, caused by shifting of the Velostat.

The **TEENSY** 3.1 ($U_{\text{input}} = 3.3$ V) and a reference resistor of 68Ω are used. The sensitivity can be changed by changing the reference resistor. The baud rate is set to 115200 bytes per second and data is collected at a sample frequency of 32 kHz. The resolution of the analog-to-digital converter (ADC) is 10 bits (0-1023). A sketch of the electric setup can be seen below in Figure 11. **ARDUINO**

software is used to extract the data from the **TEENSY 3.1** and a script in **PROCESSING 2.2.1** is written in **JAVA** to process the data. The written codes used in **ARDUINO** and **PROCESSING** software can be found in appendix C.

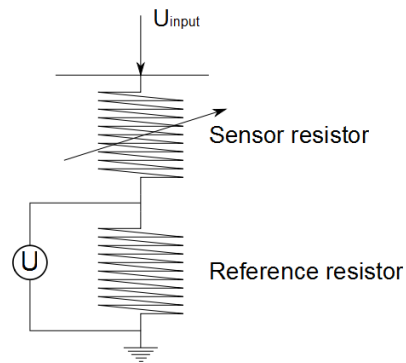


Figure 11 Electric setup

Before the drop mass is released it is important that first **CRICKETDAQ** and second **ARDUINO** are recording. For analysing dynamic compression experiments time [sec] and acceleration [m/s^2] is extracted from the acceleration sensor on the drop mass. The time [sec] and force [N] are extracted from SLS.

4. Analysis

This chapter discusses the analyses of the quasi-static and dynamic compression experiments. Further simulation of dynamic compression is explained and last section discusses the selection of foams.

4.1 Quasi-static compression

This section discusses the general analysis of quasi-static compression and subsequently the analysis of viscosity.

4.1.1 General analysis

From the **INSTRON** machine time [s], extension [m] and load [N] are extracted and together with the measured thickness [m] and area [m²] the characteristics of the foam can be analysed by using the following calculations.

The strain [-] is calculated by equation (20). In this expression $x_{\text{cut off}}$ [m] is the data which have to be removed from the beginning of the stress-strain curve. This is required for most of the foams, because of their surface roughness.

$$\varepsilon = \frac{x}{\text{thickness}}, \text{ where } x = \text{extension} - x_{\text{cut off}} \quad (20)$$

The stress [Pa] is calculated by equation (21) and smoothing of the calculated stress is required for reasons of stability. These smoothing operation is done by taking the average of nine.

$$\sigma = \frac{\text{Load}}{\text{Area}} \quad (21)$$

Further the Young's modulus [Pa] is calculated by equation (22). From this modulus the peak modulus of the linear elastic region is extracted, which is the maximum modulus of that region.

$$E = \frac{\Delta \sigma}{\Delta \varepsilon} \quad (22)$$

To determine the energy density [J/m³] equation (23) has to be solved. This is done by using the Trapezoidal rule.

$$W = \int_0^\varepsilon \sigma(\varepsilon) d\varepsilon = \sum \left(\Delta \varepsilon \frac{\sigma(a) + \sigma(b)}{2} \right) \quad (23)$$

Now the shoulder point, defined as the ratio W/σ [-], can be determined for every foam and used as the optimal point. Further the optimal strain, stress and energy at the shoulder point are useful to characterize each foam. For some structures it is required to use an adjusted shoulder point, because of a negative stiffness caused by buckling. To obtain a high (realistic) stress at the shoulder ratio, energy density is divided by the first peak stress. The differences are shown below in Figure 12.

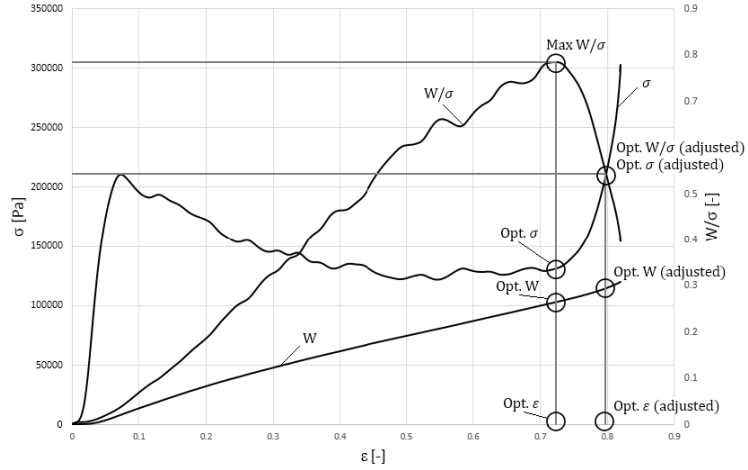


Figure 12 Adjusted shoulder point

The results of quasi-static compression experiments are used to rank all foams and structures to determine which will be tested under dynamic compression. In addition to this general analysis next section discusses the analysis of viscosity.

4.1.2 Viscosity

The viscosity parameter η gives important information about the sensitivity of strain rate dependency and is a measure of its resistance to deformations. For each foam equation (9) is used to determine its viscosity parameter. Time [sec], average stress [Pa] and strain [-] at two or three different strain rates, which differ an order of magnitude, are used to determine the viscosity parameter. An average of five strain values is used to determine the Young's modulus E [Pa]. Hereafter the Young's modulus is smoothed by an average of five as well. The strain rate [s^{-1}] is determined by equation (33).

$$\dot{\varepsilon} = \frac{\Delta\varepsilon}{\Delta t} \quad (24)$$

Next the natural logarithm of E and $(\dot{\varepsilon}_{\text{mean}} - \varepsilon)$ are taken and the complete dataset of all strain rates is sort on strain. Plotting $\ln(E)$ against $\ln(\frac{\dot{\varepsilon}_{\text{mean}}}{\varepsilon})$ the intercept and gradient of the linear regression are R and η , respectively. Only if the coefficient of determination between $\ln(\frac{\dot{\varepsilon}_{\text{mean}}}{\varepsilon})$ and $\ln(E)$, which gives the proportion of the variance of one variable that is predictable from the other variable, is higher than 80%, values of R and η are taken into account. Therefore predictions of this model can be made with a certainty of 80%. Then η is sort on increasing magnitude and negative values and extraordinary high outliers are neglected. The viscosity parameter is the mean of remaining values.

4.2 Simulation

This section discusses the simulation procedure, which is used to simulate energy absorption at higher impact energies. Therefore the distance [m], calculated by equation (20) and loading force [N], extracted from the **INSTRON** machine are needed. In this case the dimensions of each sample are not necessary. Data of the 500 mm/min compression experiments is used and is fitted by a 7th or 8th order polynomial function to obtain $F_{\text{applied}}(x)$. Then the time step is chosen to be 1 ms and then HIC_1 is marked as HIC_1 . The mass of a human head is assumed to be 5 kg. If $HIC_1 < 1000$ the desired peak acceleration is assumed to be safe. Further the initial velocity v_0 has to be set and this parameter is variable to make sure $HIC_1 < 1000$. The simulated acceleration data is extracted from the loop shown below, which is needed to calculate the overall maximum HIC_1 by using equation (10). As can be seen the trapezoidal rule is used to solve the integrals.

$x = x + \frac{v_i + v_{i-1}}{2} \cdot \Delta t$	$v = v + \frac{a_i + a_{i-1}}{2} \cdot \Delta t$
$F_{inertia} = F_{applied}(x) - F_{gravity}$	$a = \frac{F_{inertia}}{m}$

4.3 Dynamic compression

Firstly this section discusses the general analysis of dynamic compression and subsequently the analysis of SLS.

4.3.1 General analysis

The acceleration [m/s²] and time [sec] are extracted from the impact tester. A schematic overview of the setup can be seen below in Figure 13.

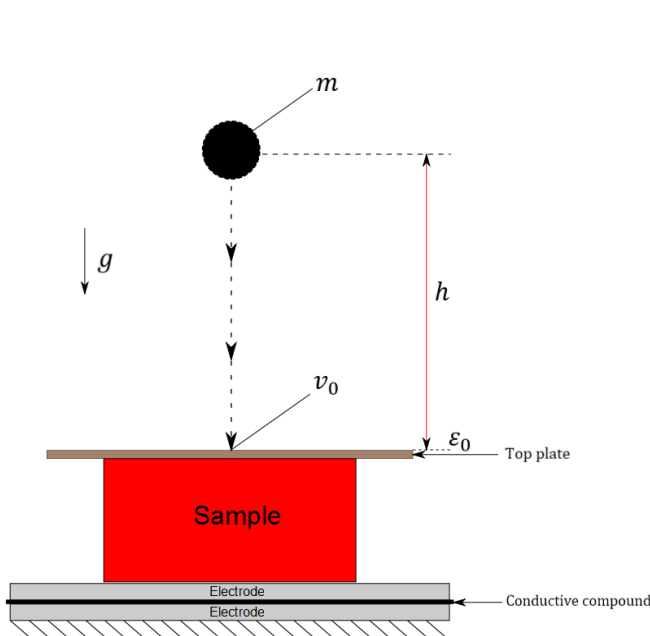


Figure 13 Test setup dynamic compression

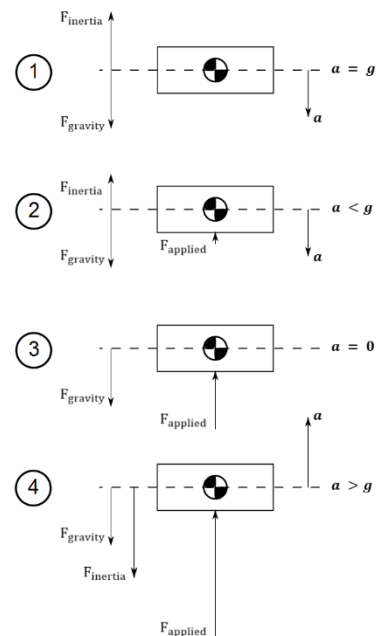


Figure 14 Four acceleration phases

The velocity of falling mass v_0 [m/s] is determined by equation (25), where h is the drop height [m] and g the standard gravity constant.

$$v_0 = \sqrt{2gh} \quad (25)$$

According to Figure 14, inertia force $F_{inertia}$ [N] is calculated by equation (26), where m is the mass [kg] and a the acceleration [m/s²].

$$F_{inertia} = ma \quad (26)$$

Four phases have been distinguished during the impact experiments, as shown in Figure 14. The first phase indicates the free fall of the drop weight. Second phase is the first moment of contact between the drop mass and sample, therefore the measured acceleration is still negative and $F_{inertia} = F_{gravity}$. In the third phase the measured acceleration is zero, which means $F_{applied} = F_{gravity}$. In the last phase the measured acceleration becomes positive and is larger than the standard gravity constant. For the last three stages, loading of the sample, yields equation (27).

$$F_{\text{applied}} = F_{\text{inertia}} + F_{\text{gravity}} \quad (27)$$

The stress σ [Pa] is calculated by dividing F_{applied} by the drop mass and from double integration of the acceleration to the time follows the travel distance x [m]. This integration is done by using the trapezoidal rule and it is important to determine exactly the times where acceleration is equal to zero, because these points are the boundaries of integration. The strain is calculated by dividing travel distance [m] by sample thickness [m]. Now the stress and strain of the loading curve are known and for calculating shoulder point, optimal stress, optimal strain and optimal energy density the same procedure as mentioned in section 4.1.1 is used.

In addition to this general analysis next section discusses the analysis of sensor less sensing.

4.3.2 Sensor less sensing

In addition to measuring acceleration from the impact tester, SLS is used to measure the force [N]. The number of bits extracted from the **TEENSY 3.1** are converted into the potential difference across the conductor U_{ref} [V] by using equation (28).

$$U_{\text{ref}} = \frac{\#bits \cdot U_{\text{input}}}{\text{Resolution}} = \frac{\#bits \cdot 3.3}{1023} \quad (28)$$

Then the current [A] can be calculated by using the Ohm law, see equation (29), where R_{ref} is the reference resistance [Ω].

$$I = U_{\text{ref}}/R_{\text{ref}} \quad (29)$$

Finally the resistance R_{Velostat} [Ω] of the conductive compound, in this case Velostat, can be calculated by equation (30).

$$R_{\text{Velostat}} = \frac{3.3 - V_{\text{ref}}}{I} \quad (30)$$

Now the sensor needs to be calibrated, which is done by using various loadings to determine the relation between R_{Velostat} [Ω] and force [N]. After these measurements the data is fitted by a power function as $\text{Force} = a \cdot R_{\text{Velostat}}^b + c$, where a , b and c are constants. Equation (31) shows the fit function and the actual fit can be seen below in Figure 15. The goodness of fit is $R^2 = 99.62$, which is assumed to be high enough for this purpose.

$$\text{Force} = 1129 \cdot R_{\text{Velostat}}^{-0.7207} - 13.53 \quad (31)$$

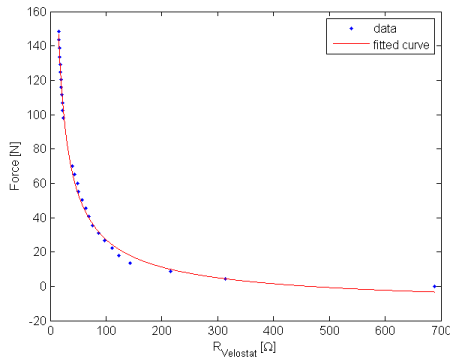


Figure 15 Calibration SLS

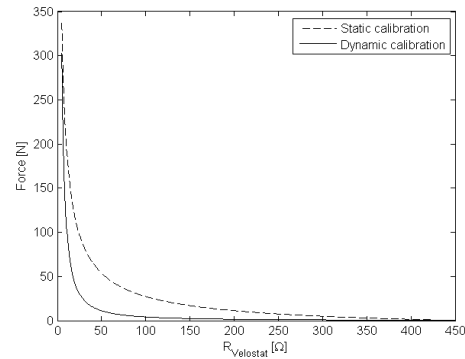


Figure 16 Static versus dynamic calibration

As a result of previous dynamic calibrations with five layers of Velostat, next calibration function is known, see equation (32).

$$\text{Force} = 3020.475 \cdot R_{\text{Velostat}}^{-1.4293} \quad (32)$$

The difference between both calibrations is shown in Figure 16. From this figure can be concluded that the dynamic calibration deals better with the visco-elastic response of Velostat. Fitting of the data is needed, because it is likely that there is not a data point exactly at the maximum force. The SLS will also be checked on top of a force plate to compare both accelerations. For this purpose a **KISTLER** Type 9260 force plate in combination with **KISTLER** Bioware Type 5691 amplifier is used. The time frame of the force plate is set to 5 seconds and the sample frequency to 17 kHz.

4.4 Selection of foams

Foams are selected by different criteria, where safety of the jockey is the most important one. Therefore the main criteria have higher priority than breathability or repeatability.

4.4.1 Main criteria

The required thickness [m] of the padding, where A is the contact area [m²], W the energy density at shoulder point [J/m³] and E_k the kinetic energy [J], is calculated by equation (33).

$$t = \frac{E_k}{W \cdot A} \quad (33)$$

The acceleration of the head is calculated by equation (34), where σ_{opt} is the stress at shoulder point [Pa] and m_{head} is the free to move mass of a head [kg].

$$a = \frac{F_{\text{opt}}}{m_{\text{head}}} = \frac{\sigma_{\text{opt}} \cdot A}{m_{\text{head}}} \quad (34)$$

To select the optimal foam based on attenuating impact energy, three criteria are used. Firstly the required thickness is less than the design thickness. Secondly the acceleration of the head is less than 300g = 2943 m/s². The free to move mass of a head is assumed to be 5 kg and the contact area as a circle with radius of 75 mm. The last criterion is HIC₁ < 1000. Then out of the feasible solutions the optimal foam is selected by minimization of density.

4.4.2 Breathability & Repeatability

The breathability of foams is an important property for reasons of thermal comfort. According to the information in section 2.9 all foams / structures are ranked in the range from one to five, where one is bad and five is good breathability. The same ranking of one to five is used for repeatability, where one is unrepeatable/unrecoverable and five fully repeatable/recoverable. Repeatability is important in case of multiple high energy impacts.

5. Results

The purpose of this research is to describe the performance and properties of different liners. In this chapter the results of all experiments are shown and in addition an expert system is developed that identifies a liner system based on a limited set of input data. This expert system will serve as a decision guide for selecting the optimal foam for specific impact scenarios.

5.1 Quasi-static compression

First this section discusses general results of quasi-static compression. This is followed by more specific results, like combined performance, viscosity and comparing shoulder points.

5.1.1 General results

All experiments are performed and analysed according to the procedure described in previous chapters. The optimal energy absorption diagram, shoulder point versus optimal strain, can be seen below in Figure 17. The density of the foams/structures is an important parameter as well, because one of the requirements is a lightweight design. Therefore the relation between shoulder point versus density is investigated and can be seen in Figure 18. Naturally, the higher the density, the stronger and harder the foam is.

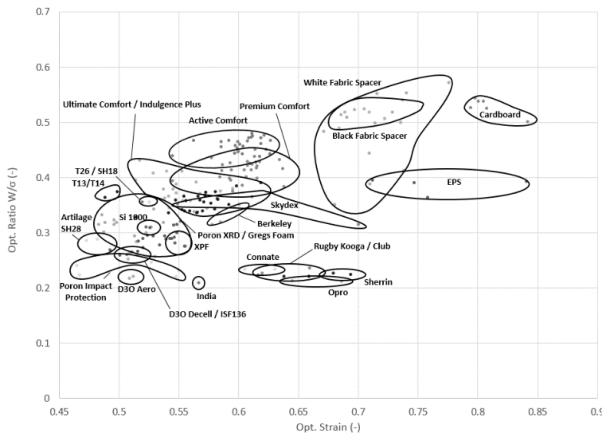


Figure 17 Shoulder point versus optimal strain

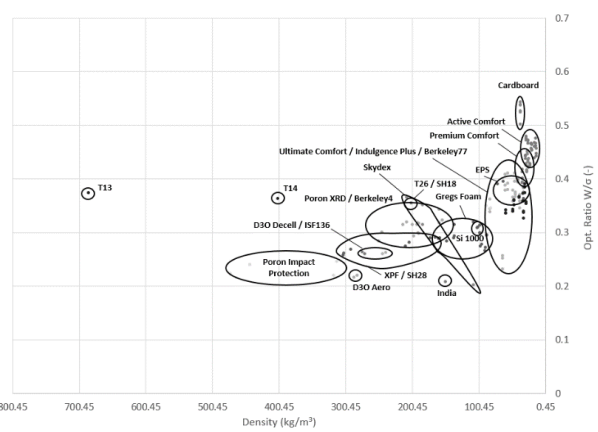


Figure 18 Shoulder point versus density

From the graphs follow that cardboard has the best performance, because it is lightweight and has a high shoulder point. Further can be seen that EPS and Fabric Spacer have also good energy absorption properties. It is clear that many of the tested materials have bad performances and it make sense that most structures have higher densities than foam, except for cardboard. According to section 2.6 it was expected that the optimal strain of foams is between 45% and 68%.

Since not only the shoulder point determines its performance, but the optimal energy density is of importance as well, Figure 19 shows the optimal energy density versus the optimal stress on a double log scale.

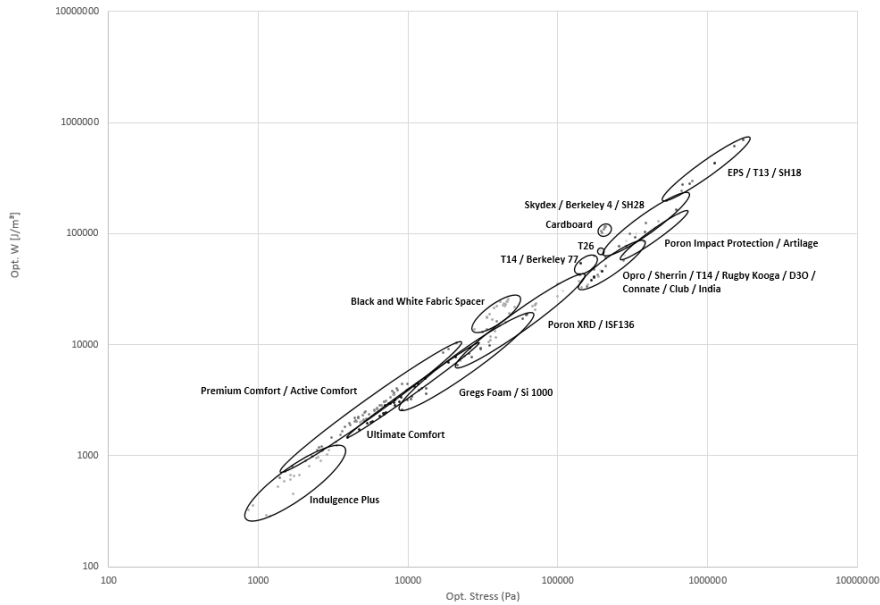


Figure 19 Optimal energy density versus optimal stress

From above figure follows that EPS, T13 and SH18 have a high optimal energy density, which means they can absorb a large amount of energy. Skydex, Poron Impact Protection and Artilage have also high optimal energy densities in contrast to all comfort foams like Active Comfort, Premium Comfort, Ultimate Comfort and Indulgence Plus. Further the optimal stress versus optimal strain is investigated and can be seen below in Figure 20, where the optimal stress is plotted on log scale.

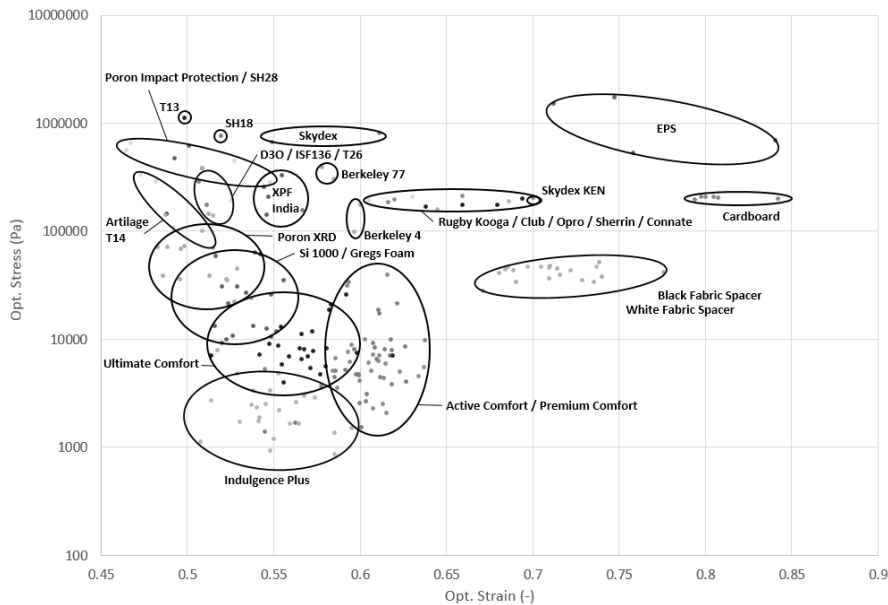


Figure 20 Optimal stress versus optimal strain

From this figure can be concluded that all comfort foams like Active Comfort, Premium Comfort, Ultimate Comfort and Indulgence Plus have a low optimal stress and optimal strain. Foams/structures at the same optimal stress may be used to design an energy absorbing comfort layer. In general absorbing characteristics of composites are worse, therefore this is not recommended. For the purpose of this research it is advisable to select the best impact absorbing material and on top of that it is possible to add a thin comfort layer.

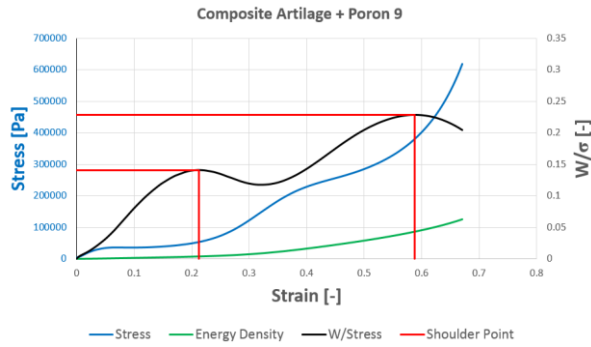


Figure 22 Result Composite

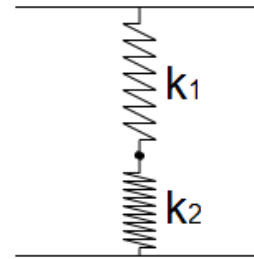


Figure 23 Model composite

For the composite two shoulder points can be obtained as there are two different foams. The shoulder points are at 0.14 and 0.23, where the lower corresponds to Poron XRD 9 and the higher to Artilage.

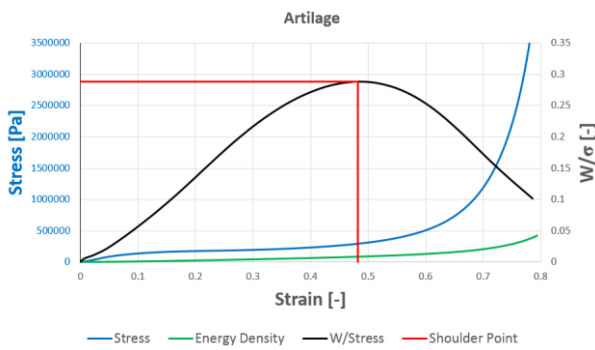


Figure 24 Result Artilage

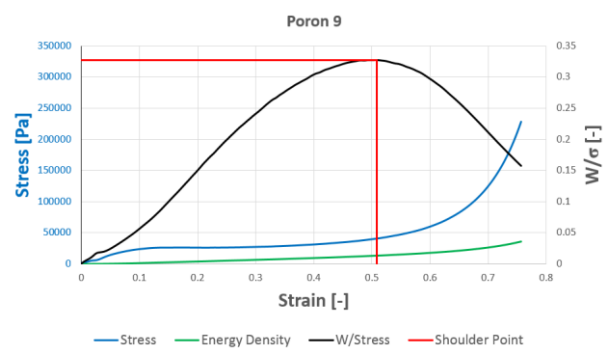


Figure 25 Result Poron XRD 9

In case of separated materials the shoulder points are at 0.29 and 0.33 for Artilage and Poron XRD 9, respectively. This behaviour can be explained by taking an equivalent stiffness for the composite, according to the model in Figure 23. The equivalent stiffness is calculated by equation (35) and it is clear that $k_{eq} < k_1 < k_2$, if $k_1 < k_2$.

$$k_{eq} = \frac{1}{\left(\frac{1}{k_1}\right) + \left(\frac{1}{k_2}\right)} \quad (35)$$

Lower stiffness means more strain at the same force, which leads to a lower shoulder point. It is clear that the shoulder point of a composite is always lower than the shoulder points of its separated materials.

5.1.3 Viscosity

The viscosity parameters are calculated according to section 4.1.2 and can be seen below in Figure 26.

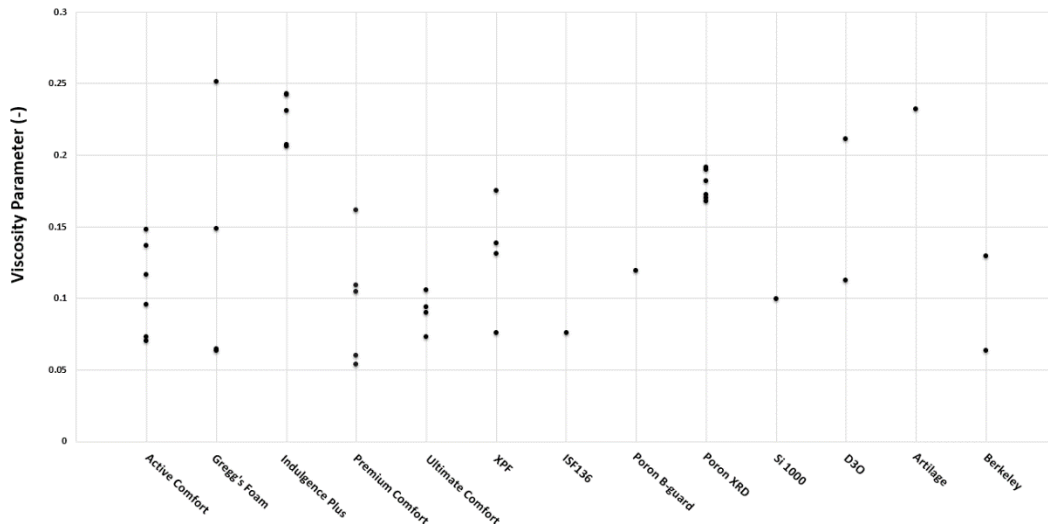


Figure 26 Viscosity parameters

From the graph can be concluded that most foams are in the range of 5-15% viscous and the memory foams in the range of 20-25%. The Poron XRD foams are in the range of 15-20% viscous, so they are slightly less viscous than the memory foams. Further can be seen that D30 Aero is more viscous than D30 Decell, where the first one is a memory foam. These viscosities are as expected, except for Greggs Foams Purple. The reason for this outlier is found in the fact that this viscosity parameter is only the mean of 6 values, which is not enough for a good approximation.

5.1.4 Shoulder points

The shoulder points of four closed-cell foams are compared in Figure 27 and as shown they are on a straight envelope. This is different than previously thought, see section 2.5, because for closed-cell foams the shoulder points are expected to be on a curved envelope.

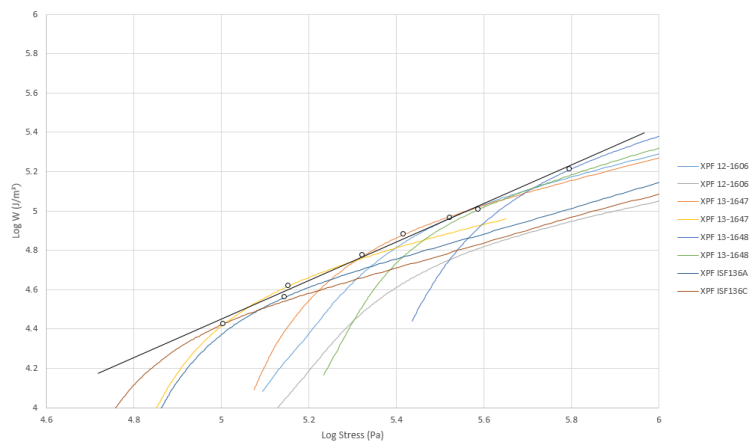


Figure 27 Shoulder points

For closed-cell foams yield at high densities that cell-wall deformation is the dominant energy-absorbing process instead of compression of the gas within the cells. The reason that the shoulder points of the four investigated foams, shown in Figure 27, are at a straight envelope is because they have high densities. Therefore these foams behave like an open-cell foam, where the buckling of the cell-walls is the dominant energy-absorbing process.

5.1.5 Case study company results

Albion has performed some impact experiments with Artilage and B-guard in combination with the helmet shell and their results are compared to the results of quasi-static compression. Albion

has tested with three different drop masses, namely 4.1 kg, 4.7 kg and 5.6 kg. Their results are shown in Table 1, where also the energies [J] are calculated for each mass in combination with a specific drop height. An acceleration less than 300g is assumed to be safe.

Albion claimed that a combination of B-guard and Poron XRD 09 was not suitable to pass the ARB requirements (2.5 m drop), however it had satisfactory results when tested at AS/NZ standard (1.5 m drop) and the ARB hazard anvil requirements (2.0 m drop on a V-shaped hazard anvil). Only two liner combinations passed the ARB requirements (2.5 m drop), namely SH28 and SH18 of 13.5 mm thickness at 115 J. However it failed to replicate this performance to the other impact energies, indicating the performance could not be simply scaled. Further it is claimed that SH18 performed better than SH28 and SH18 can be a working solution for 115 J at a thickness of 13 mm [21].

Table 1 Results Albion – acceleration

	Thickness [mm]	1.5 m			2.5 m		
		E = 60 J	E = 69 J	E = 82 J	E = 100 J	E = 115 J	E = 137 J
SH18	10		216g				
SH18	13				357-384g	186-363g	
SH28	7.5		334g				
SH28	10		237g				
SH28	13.5				248-412g	209-285g	
B-guard	15	188-412g	172g	183-322g	367-538g	317-722g	320-479g

The results for SH18, SH28 and B-guard of the quasi-static compression experiments can be seen below in Table 2 and Table 3. These tables show the required layer thickness [mm] to absorb the impact energy, which is calculated by equation (33) and the acceleration [g] of a human head, calculated by equation (34). These results are only valid for a specific thickness, which is the sample thickness, but they give a good indication of the foam characteristics. Furthermore, the comfort layer, Poron XRD 09 in the experiments of Albion, is not taken into account due to its bad energy-absorbing characteristics.

Table 2 Required layer thickness

	1.5 m			2.5 m		
	E = 60 J	E = 69 J	E = 82 J	E = 100 J	E = 115 J	E = 137 J
SH18	12 mm	14 mm	17 mm	21 mm	24 mm	28 mm
SH28	27 mm	30 mm	36 mm	44 mm	51 mm	61 mm
B-guard	30 mm	35 mm	42 mm	51 mm	58 mm	70 mm

Table 3 Acceleration quasi-static compression

	Acceleration head
SH18 at t = 13 mm	277.7g
SH28 at t = 13.3 mm	171.8g
B-guard at t = 14.1 mm	162.6g

By comparing both results, it can be concluded that most outcomes of Albion are as expected. First it can be seen that the required thicknesses of SH18 is less than SH28, which means that SH18 has a higher optimal energy density. Albion claimed this better performance of SH18 as well. It is likely that a layer of SH18 of 13 mm would be enough for absorbing 60 J, but unfortunately this is not investigated by Albion. Further can be seen that many liner combinations are not safe enough, which means their accelerations are too high in combination with their thickness. As shown in Table 3, the acceleration of a human head would be less while using B-guard, because the optimal stress of B-guard is higher. This behaviour can be seen in Table 1 as well. However, there is a large

variance in the results of Albion, which makes it hard to draw valid conclusions. The acceleration of a human head while using SH28 is less than using SH18, due to the lower optimal stress of SH28. Therefore SH28 would be a safer solution than SH18 even though this requires a thicker layer. Finally from both results can be concluded that it is not possible to scale these foams simply. The impact absorbing characteristics are dependent on both the optimal energy density and optimal stress, therefore only scaling via the shoulder point is possible.

5.2 Simulation

All simulations are performed and analysed according to the procedure described in chapter 4.1.2 to simulate the energy-absorption characteristics at higher impact energies. In these simulations viscosity effects are not taken into account. The shoulder point [-] versus maximum simulated initial velocity [m/s] can be seen below in Figure 28.

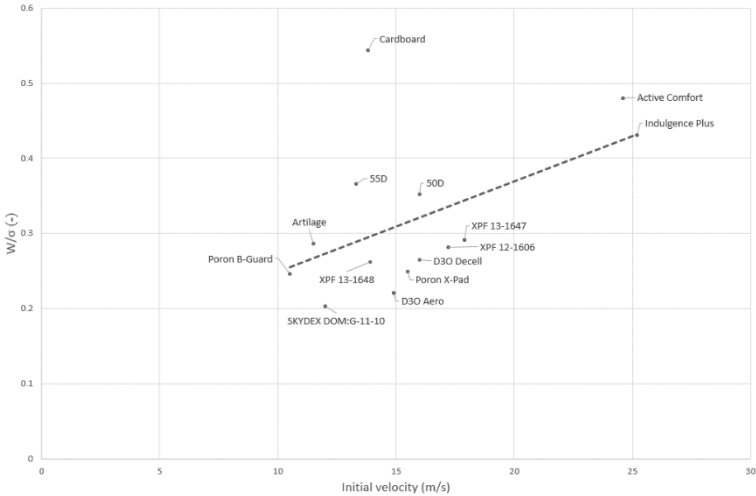


Figure 28 Shoulder point versus simulated maximum initial velocity

As can be seen in the figure the higher the shoulder point, determined by quasi-static compression, the higher the simulated initial velocity. This trend is indicated by the black dotted line. This makes sense, because the higher the initial velocity at $HIC_1 < 1000$, the higher the absorbed impact energy and therefore the better the impact energy-absorption characteristics. There is one outlier, namely Cardboard. This outlier is because of the model for force-extension data, because it has a negative stiffness at some point in the loading curve, which made it hard to obtain a good fit. In short can be concluded that quasi-static compression results are useful to simulate impact characteristics, although visco-elastic effects have more influence at higher impact energies, which means an increase of impact absorbing characteristics.

5.3 Dynamic compression

This section discusses the results of the impact tester and subsequently the results of SLS compared to the force plate.

5.3.1 Impact tester

All dynamic compression experiments are performed and analysed according to previous chapters and the results can be found in this section. First Figure 29 shows the shoulder point versus optimal strain.

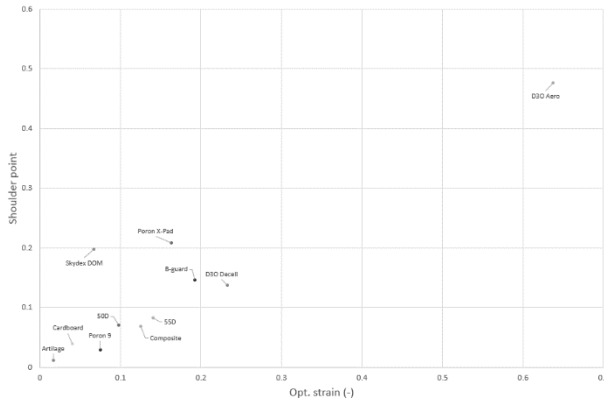


Figure 29 Shoulder point versus optimal strain

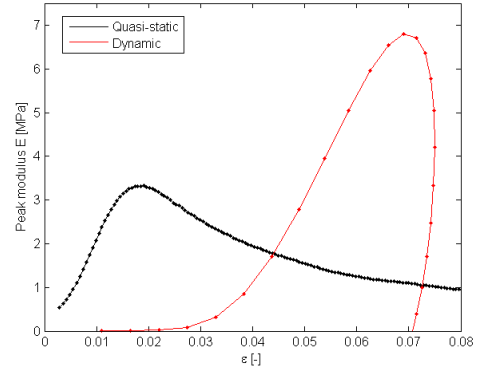


Figure 30 Peak modulus

As expected the shoulder points and optimal strains are less than found by quasi-static compression due to stiffening of the samples. This is caused by the higher peak modulus during dynamic compression, as shown above in for Artilage at an impact energy of 19.8 J. In general, the higher the impact energy, the higher the peak modulus and the lower the calculated shoulder point.

However, the calculated shoulder points are far lower and this is probably caused by double integration from acceleration to distance in combination with the increase in velocity during the first contact between drop mass and sample. This is explained below in Figure 31, which yields also for Artilage at an impact energy of 19.8 J. Here, acceleration is taken positive downwards and consequently the initial velocity is negative and becomes positive.

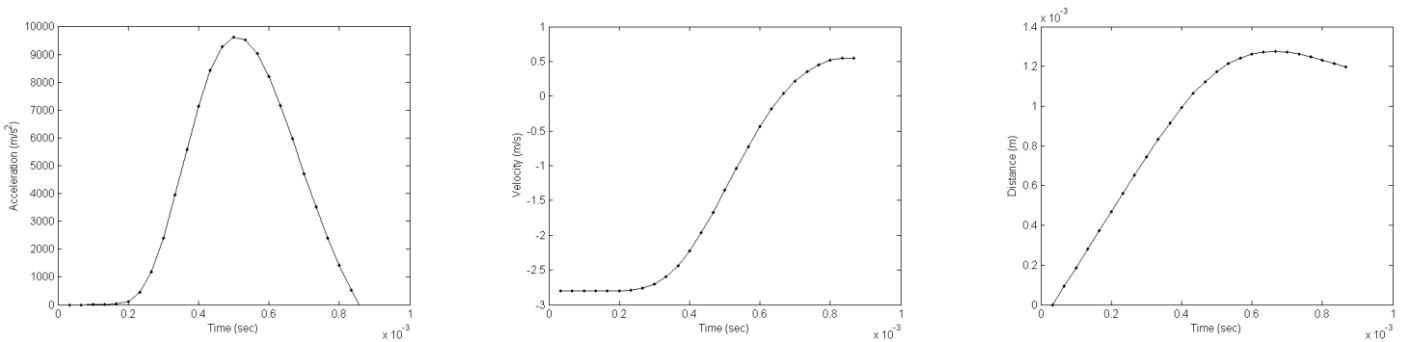


Figure 31 Double integration

As a result of integration the velocity is maximum at zero acceleration (after the impact) and the travel distance is maximum at zero velocity. It can be seen that during the first moment of impact the velocity is still slightly decreasing and negative. Hereafter it becomes positive, but after some time it decreases constantly due to the negative acceleration of the standard gravity constant. In short, it is possible to use double integration, but then by fitting the acceleration data, which means each single peak needs a fit function and hereafter double integration to the time. This is done for cardboard.

For cardboard the maximum strain is investigated as well by measuring the thickness before and after the impact. This is summed up below in Table 4 and yields for an impact energy of 49 J (drop height: 1m), which is enough to reach densification region.

Table 4 Measured thickness cardboard

	Before impact	After impact
Thickness [mm]	18.6	4
Strain [%]	0	78.5

The acceleration data from the impact tester is fitted by a sixth order polynomial function. For this purpose each single acceleration peak is fitted by another function to take into account all bounces after the first impact, because these bounces have influence on the final thickness of this cardboard sample. All obtained fit functions are integrated twice to get the distance. The first integration constant is the initial velocity, which is $v_0 = 4.43 \text{ m/s}$ and this constant is adapted for every following bounce. The theoretical distance is 11 mm, which results in 59.1%. This strain is less than measured from the cardboard sample and can be explained by the following considerations. First the actual (measured) drop height can be slightly different, and therefore the initial velocity is different. Further theoretical the impact is considered as two-sided loading, while in real the impact is one-sided. Last cause of this difference is the error made by fitting the acceleration data. However, the theoretical is close to the actual strain (percentage error of 25%) and therefore this theoretical approach can give more insight into other samples.

To prevent double integration from acceleration to distance for calculating the strain, the impact energy density $W \text{ [J/m}^3\text{]}$ is divided by the peak stress $\sigma_{\text{peak}} \text{ [MPa]}$. Many experiments are performed with cardboard, D30 Aero and Poron 15500 at different drop heights to investigate their shoulder points at various impact energies. The results, shoulder point versus peak stress $\sigma_{\text{peak}} \text{ [MPa]}$, can be seen below in Figure 32.

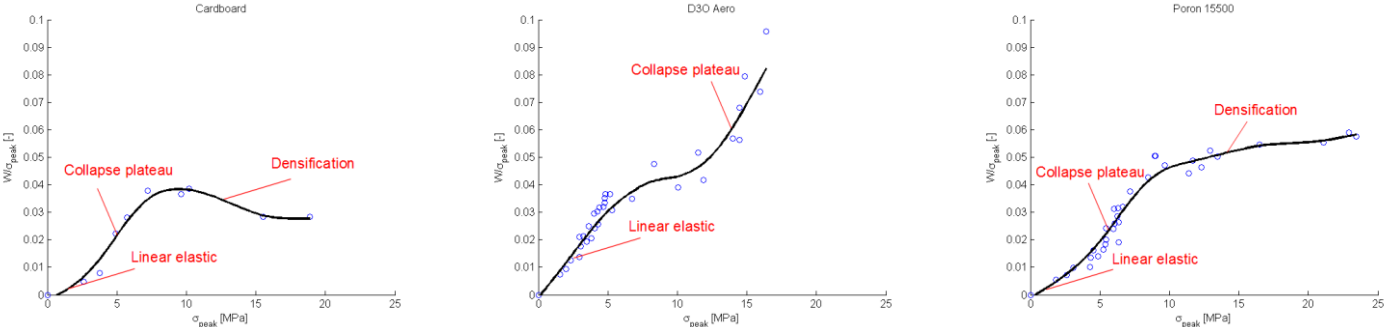


Figure 32 Comparison between cardboard, D30 Aero and Poron 15500

From Figure 32 can be concluded that only cardboard and Poron 15500 reach densification. D30 Aero will never reach densification, because of shear thickening. Shear thickening, also known as dilatant, is a time-independent increase in viscosity; the apparent viscosity increases with increased stress (and shear rate). It is clear that it is impossible to calculate the shoulder point if D30 Aero do not reach densification. For materials without shear thickening these results can be used to determine their impact energy absorption.

Pictures of cardboard after an impact of 0.69 J can be seen below in Figure 33. The energy is absorbed in the linear elastic region by buckling of cell walls.

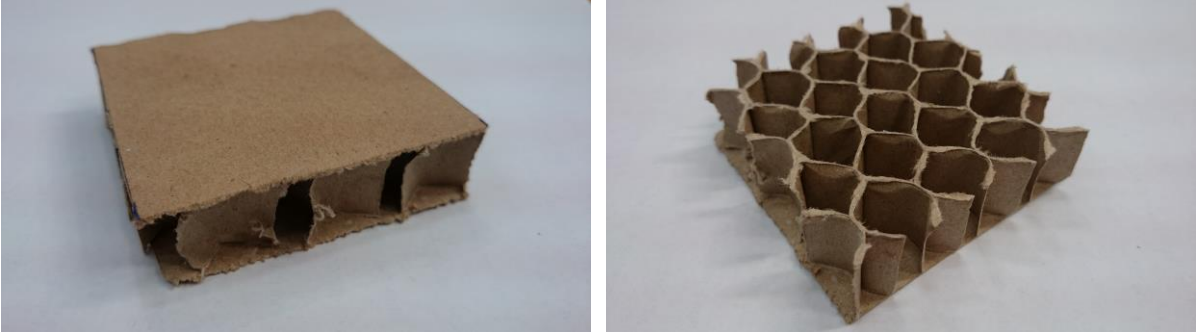


Figure 33 Result cardboard 1.19 J

From the pictures of cardboard can be concluded that buckling occurred in a few cell walls, but most cell walls are deformed elastically.

Further the effect of doubling thickness or area is investigated. Experiments are performed with samples of D30 Aero and Poron 15500 and their results can be seen in Figure 34 and Figure 35, respectively. It is expected that the slope of double thickness is 0.5 times the slope of single sample and with equal impact energy σ_{peak} of double area is 2 times the σ_{peak} of single sample.

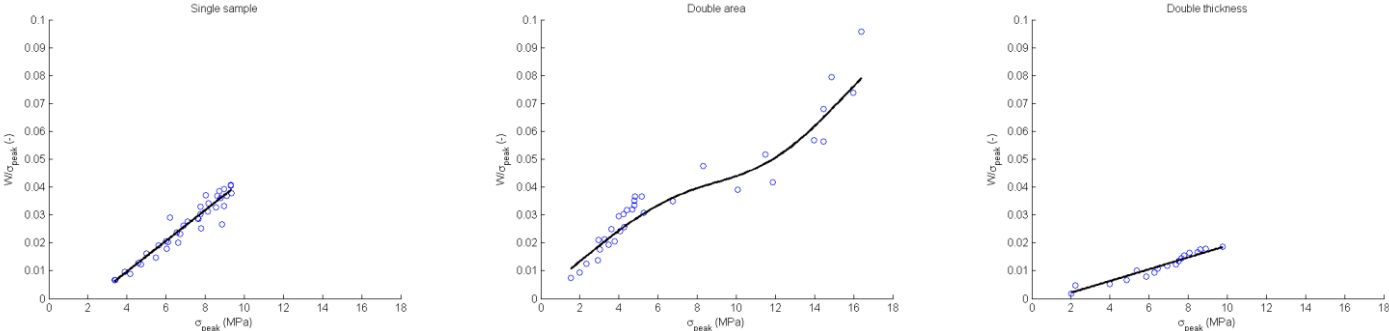


Figure 34 Scaling D30 Aero

In case of D30 Aero can be calculated that the slope of double thickness is 0.44 times the slope of single sample and with equal impact energy σ_{peak} of double area is 2.27 times the σ_{peak} of single sample.

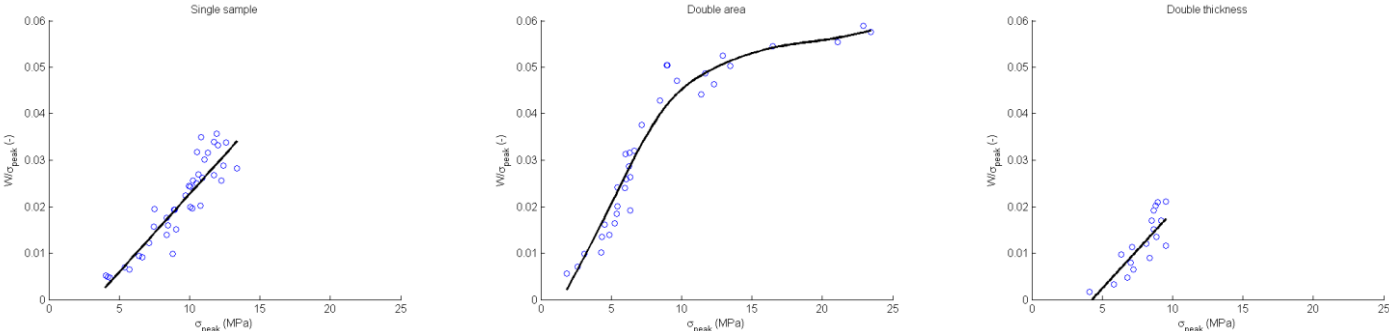


Figure 35 Scaling Poron 15500

In case of Poron 15500 can be calculated that the slope of double thickness is 0.70 times the slope of single sample and with equal impact energy σ_{peak} of double area is 1.55 times the σ_{peak} of single sample. From both materials can be concluded that their behaviour is as expected, however the error of Poron 15500 is larger. Most likely this error is caused by the dimensions of the samples, for example in case of double thickness the aspect ratio thickness/area is not optimal.

5.3.2 Sensor less sensing

The results of SLS are compared to the force plate and this comparison can be seen below in Figure 36. This figure shows acceleration [m/s²] versus time [sec] for SLS and force plate. The data of the force plate is converted into acceleration by the mass.

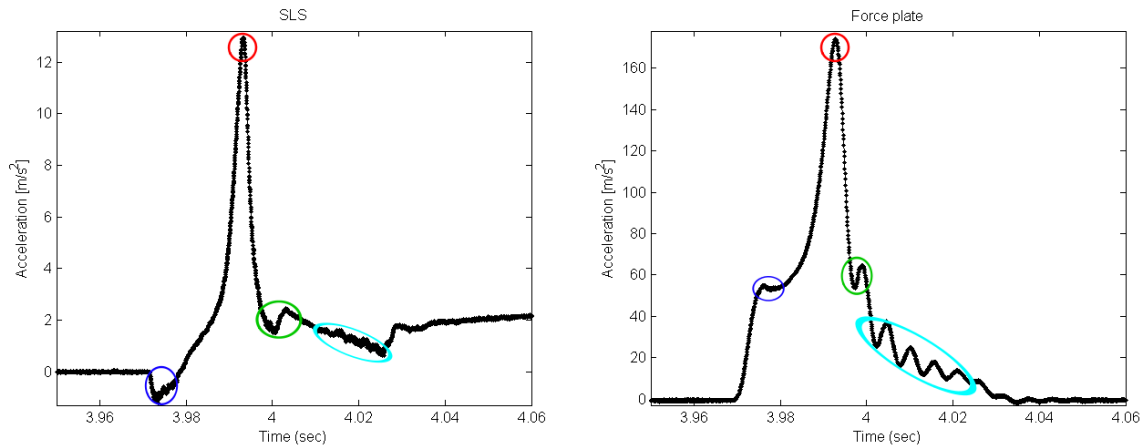


Figure 36 Comparison SLS and force plate

The result of SLS is very similar to that of the force plate, although the peak acceleration of SLS is far less than measured by the force plate, this is 12.8 m/s^2 and 172.8 m/s^2 , respectively. This difference is probably caused by the static calibration of SLS; there are probably visco-elastic effects. When the dynamic calibration of SLS is used, see equation (32), an acceleration peak of $3.53 \cdot 10^4 \text{ m/s}^2$ is obtained, which is much higher than the peak measured by the force plate.

Further every result of SLS shows a valley before the peak acceleration, mentioned by the blue circle. It is not clear how this influences the maximum peak acceleration, and it is probably caused by captured air between the Velostat layers. During the first moments of the impact captured air is pushed out and therefore the resistance of the sensor becomes a bit more, which results in less acceleration. However this behaviour is dependent on the impact energy, which means that it is hard to compensate for this behaviour. From the figure can be concluded that both SLS and force plate measures the drop weight after the impact and the unloading of SLS is slower than that of the force plate, which is mentioned by green and turquoise circles.

In short can be concluded that SLS did not work properly and it is unclear whether it measures the right peak acceleration or not. SLS is not optimized in this research, because it is in addition to the acceleration sensor of the impact tester.

5.4 Design guide

An important outcome of this research is a design guide for the company. The design guide is based on quasi-static compression, because at the moment of writing not all impact results are known. The selection of impact padding is based on the main criteria, which can be found in section 4.4 and requires the following input parameters:

- Impact energy [J]
- Contact area [m^2]
- Maximum allowable thickness [m]
- Mass head [kg]

The outputs of the design guide are the first six possible solutions, which means that acceleration of the head is less than 300g and the required thickness is less than allowed thickness. These feasible solutions are sorted on increasing density to design lightweight. An example of using the design guide can be seen below in Figure 37.

DESIGN GUIDE									
Input:	Impact Energy (J)	Contact Area (m ²)	Max allowed thickness (mm)	Mass head (kg)					
	200	0.017671459	0.1	5					
Output:	Foam	Opt. Ratio	Required thickness (mm)	Density (kg/m ³)	Breathability (bad - good, 1-5)	Repeatability (bad - good, 1-5)	Type of foam	Remarks	Number of possible solutions
Optimal solution:	EPS White (White1)	0.364140904	0.057882473	33.84395425	4	1	Structure	This material is not recoverable	12
Second solution:	EPS White (White2)	0.393537238	0.041539571	35.25173611	4	1	Structure	This material is not recoverable	
Third solution:	Cardboard (CB4)	0.543718362	0.098962664	38.70967742	3	1	Structure	This material is not recoverable	
Fourth solution:	50D (50A)	0.352468741	0.047456287	185.0949365	3	3	Structure		
Fifth solution:	SH18 (SH18)	0.356071037	0.041229758	202.8014926	2	4	Reticulated	Bad breathability	
Sixth solution:	55D (55A)	0.36586497	0.038400214	209.0717736	3	3	Structure		

Figure 37 Design guide

For reasons of flexibility and more insight in the possibilities several outcomes are given by this design guide. First is given the optimal solution, which means a feasible padding with the lowest density. Next solutions are sorted on increasing density and also the total number of feasible solutions can be seen. Remarks are shown as the breathability ≤ 2 or repeatability ≤ 2 . For these input parameters the optimal solution is EPS White, but if the customer wants a recoverable material they can better choose for 50D.

The results of dynamic compression are not included in this design guide, because at the moment of writing more impact experiments are required. However, the outcomes of quasi-static compression give an good insight in the behaviour of each material. The jockey helmet padding is designed to absorb impact energy. On top of this padding a thin soft layer can be used to increase the comfort for the jockey. This comfort layer is out of the purpose of this research.

6. Conclusions and Discussion

Summary of what was found in previous chapters. First important conclusions are discussed and subsequently some discussion topics are mentioned.

6.1 Conclusions

An important, independent, parameter in designing an impact layer is the shoulder point. This ratio W/σ can be used to select and optimize various foams and structures. In addition to the shoulder point density is important to design lightweight. From the quasi-static compression can be concluded that cardboard has the best performances. Further the optimal energy density is an important design parameter, because it determines the amount of absorbed energy at the shoulder point. All investigated materials show strain rate dependency, which means that they can absorb more energy at higher strain rates. Combined performance of an impact layer in combination with a soft comfort layer is always worse, because the equivalent stiffness is less than both separate stiffness's. On top of this padding a thin soft layer can be used to increase the comfort for the jockey. The case study of impact experiments of Albion shows that their results could be expected. This shows that quasi-static results give a good insight in the impact absorbing characteristics of all materials. In addition simulations of higher impact energies from quasi-static compression data showed expected characteristics.

In case of dynamic compression experiments low shoulder points are found, as a result of high peak moduli. Moreover, acceleration data extracted from the impact tester could not be integrated twice to get the travel distance. To avoid double integration impact energy density is divided by the peak stress to investigate impact characteristics of each material. It can be concluded that more dynamic compression experiments and research have to be done to finalize and optimize the design guide for jockey helmets.

Sensor less sensing (SLS) did not work properly and it is unclear whether it measures the right peak acceleration or not. SLS is not optimized in this research, because it is in addition to the acceleration sensor of the impact tester.

The safety of jockeys has high priority, so therefore the padding must be designed on HIC less than 1000 and acceleration of a human head less than $300g$, where g is the standard gravity constant. The design guide is based on quasi-static results to select and design jockey helmets. It shows the six best solutions sorted on increasing density to design lightweight, where the required layer thickness is less than the allowable layer thickness.

6.2 Discussion

Firstly in the main safety criteria rotational acceleration of a human brain is not taken into account. This can cause concussion as well.

Further foams will react different while they are wet. It can be raining during a game or the jockey is sweating. The effects of water should be taken into account in selecting the impact padding.

To rank the materials the contact area is assumed to be a circle with a radius of 75 mm. This contact area depends on design of the jockey helmet and must be adjusted when the design is known.

7. Recommendations

Based on conclusions made in this report some recommendations for further research are discussed in this chapter.

Firstly, based on the performance of cardboard, it is highly recommended to use this hexagon structure as impact absorber. The hexagon structure can be made easily by using techniques like additive manufacturing (3D printing).

Secondly it is recommended to optimize SLS to make it useful for measuring further experiments. It is important to know how Velostat responds to impacts and it should be calibrated for this dynamic compression. Because of its visco-elastic respond the SLS must be calibrated on a force plate. Further to prevent

Thirdly it is recommended to investigate the breathability of each foam / structure. Only the distinguish between open-cell, closed-cell and reticulated foams is taken into account in this research. More research is needed to determine the air flow and porosity of each foam / structure. Porosity can be measured by, for example, dropping the foam into water and measure its solid weight.

Fourthly it is recommended to verify the derivation of open-cell and closed-cell foams, which can be found in section 2.6. For open-cell foams this can be done by testing a fixed-fixed and pinned-pinned supported slender rod in compression. For closed-cell foams experiments with a pneumatic cylinder can be performed to measure its optimal strain at shoulder point.

Last recommendation is to investigate other lightweight impact absorbing structures, like sandwich structures. Sandwich structures with a foam core could be useful for jockey helmets.

8. Bibliography

- [1] Albion (2014). *Our story* [online]. Available at: <http://www.albionsports.com/page/our-story> [Accessed 25 September 2014]
- [2] Ashby, M. F. (1989). *Overview No. 80: On the engineering properties of materials*. Acta metallurgica, 37(5), 1273-1293.
- [3] Wikipedia (2014). *Foam* [online]. Available at: <http://en.wikipedia.org/wiki/Foam> [Accessed 25 September 2014]
- [4] Foam-Tech (2008). *What is the Difference Between Open-cell and Closed-cell Polyurethane Foams?* [online]. Available at: <http://www.foam-tech.com/products/urethane-foam/open-closed-cell.htm> [Accessed 23 September 2014]
- [5] Gibson LJ, Ashby MF. *Cellular solids - structure and properties*, 2nd ed. Cambridge: Cambridge University Press; 1997
- [6] Jain V, Johnson I, Ganesh I, Saha BP, Mahajan YR. *Effect of rubber encapsulation on the comparative mechanical behaviour of ceramic honeycomb and foam*. Mater. Sci. Eng. A. 2003; 347; 109-122.
- [7] Avalle, M., Belingardi, G., & Montanini, R. (2001). *Characterization of polymeric structural foams under compressive impact loading by means of energy-absorption diagram*. International Journal of Impact Engineering, 25(5), 455-472.
- [8] Avalle, M., Belingardi, G., & Ibba, A. (2007). *Mechanical models of cellular solids: Parameters identification from experimental tests*. International Journal of Impact Engineering, 34(1), 3-27.
- [9] Rusch KC. *Load-compression behaviour of brittle foams*. J. Appl. Polymer Sci. 14, 1263-1276.
- [10] Ouellet, S., Cronin, D., & Worswick, M. (2006). *Compressive response of polymeric foams under quasi-static, medium and high strain rate conditions*. Polymer testing, 25(6), 731-743.
- [11] Vesenjok M, _uni_ Z, Öchsner A, Hriber_ek M, Ren Z. *Heat conduction in closed-cell cellular metals*. Mater. Sci. Eng. Tech. 2005; 36, (10): 608-612
- [12] Nagy, A., Ko, W. L., & Lindholm, U. S. (1973). *Mechanical Behavior of Foamed Materials under Dynamic Compression*. Southwest research inst san antonio tex.
- [13] Mills, N. (2007). *Polymer foams handbook: engineering and biomechanics applications and design guide, page 92*, Butterworth-Heinemann.
- [14] Fuss, F. K. (2012). *Nonlinear Visco-Elastic Materials*. In *Nonlinear Approaches in Engineering Applications* (pp. 135-170). Springer New York.
- [15] Hibbeler, R.C. (2011). *Mechanics of Materials*. Pearson Prentice Hall
- [16] Megson, T. H. G. (2013). *Introduction to Aircraft Structural Analysis*. Butterworth-Heinemann.
- [17] Henn, H. W. (1998). *Crash tests and the head injury criterion*. Teaching mathematics and its applications, 17(4), 162-170.
- [18] McIntosh, A. S., & McCrory, P. (2000). *Impact energy attenuation performance of football headgear*. British journal of sports medicine, 34(5), 337-341.
- [19] Wikipedia (2014). *Piezoresistive effect* [online]. Available at: http://en.wikipedia.org/wiki/Piezoresistive_effect [Accessed at 23 October 2014]
- [20] Liu, C. (2012). *Foundations of MEMS*. Pearson Education India.
- [21] M. Kajtaz (2014) *Liner Development, In Situ Testing 2 – Internal Report*. Albion Sports

Appendix A – Derivation open-cell

This appendix discusses the derivation of the optimal strain at shoulder point for open-cell foams and is complement to section 2.6.1 of the main report.

The structure of open-cell foams is modelled like buckling of a slender rod. A distinction is made between pinned – pinned and fixed – fixed support, as shown below in Figure 38.

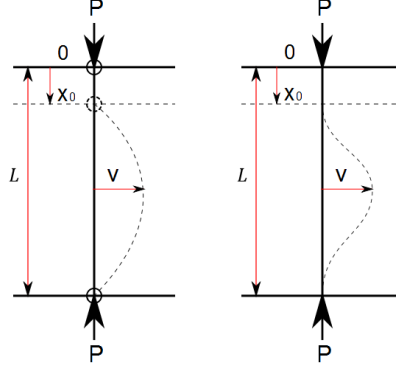


Figure 38 Models open-cell foam
(left is pinned-pinned support, right is fixed-fixed support)

In general for buckling of an Euler beam, in the first buckling mode ($n = 1$), the critical load is defined as equation (36), where K is a correction factor for the support type.

$$P_{\text{crit}} = \frac{n^2 \pi^2 EI}{(KL - x_0)^2} = \frac{\pi^2 EI}{(KL - x_0)^2} \quad (36)$$

Then the deflection v is described as equation (37) [15].

$$v = v_{\text{max}} \sin\left(\pi \frac{(x - x_0)}{(KL - x_0)}\right) \quad (37)$$

The second derivative to x is described in equation (38) [16]:

$$\frac{d^2 v}{dx^2} = \frac{M}{EI} = -\frac{vP}{EI} \quad (38)$$

Substitute for $\frac{P_{\text{crit}}}{EI} = \frac{\pi^2}{(KL - x_0)^2}$:

$$\frac{d^2 v}{dx^2} = -v_{\text{max}} \left(\frac{\pi^2}{(KL - x_0)^2}\right) \sin\left(\pi \frac{(x - x_0)}{(KL - x_0)}\right) \quad (39)$$

At v_{max} : $x = \frac{L - x_0}{2}$

$$-\frac{vP_{\text{crit}}}{EI} = -v_{\text{max}} \left(\frac{\pi^2}{(KL - x_0)^2}\right) \sin\left(\pi \frac{L - 3x_0}{2KL - 2x_0}\right) \quad (40)$$

$$E_b = \int P_{\text{crit}} dx_0 = EI \left(\frac{\pi^2}{KL - x_0} - \frac{\pi^2}{KL}\right) \rightarrow \frac{E_b}{P_{\text{crit}}} = \frac{x(KL - x)}{KL} \quad (41)$$

Max gradient: $\frac{d}{dx} \left(\frac{E_b}{P}\right) = 1 - \frac{2x}{KL} = 0 \rightarrow x = \frac{KL}{2}$. Then $P_{\text{max gradient}} = EI \left(\frac{2\pi}{KL}\right)^2$

Assume that v_{\max} is at $x = \frac{KL}{2}$, then in case of pinned-pinned yields $K = 1$, which means $\varepsilon_{\max} = \frac{L/2}{L} = 0.5$. In case of fixed-fixed yields $K = 0.5$, which means $\varepsilon_{\max} = \frac{L/4}{L} = 0.25$. So that turns out that for open-cell foams the optimal strain at shoulder point is at least 0.25.

Appendix B – Derivation closed-cell

This appendix discusses the derivation of the optimal strain at shoulder point for closed-cell foams and is complement to section 2.6.2 of the main report.

For closed-cell foams a different model is needed, because of the compression of the enclosed gas. This calculation uses the model defined by Rusch [9], as shown in Figure 5.

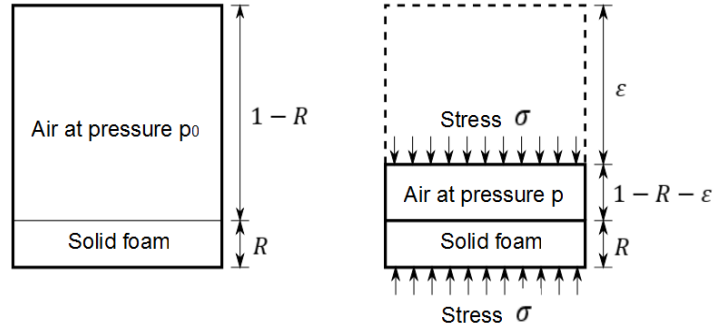


Figure 39 Model closed-cell foam

Assumed that there is no lateral expansion, which means the Poisson ratio is zero, the volumetric strain is equal to the compressive strain, isothermal gas compression and incompressible foam walls, then yields according to Figure 5 equation (42), where R is the relative density: $R = \rho^*/\rho_s = 1 - P$.

$$p_0(1 - R) = p(1 - R - \varepsilon) \quad (42)$$

The stress becomes as equation (43).

$$\sigma_g = p - p_0 = p_0 \frac{\varepsilon}{1 - \varepsilon - R} \quad (43)$$

Further the energy density of the compressed gas can be described by equation (44).

$$W_g = p_0 \int_0^\varepsilon \frac{\varepsilon}{1 - \varepsilon - R} d\varepsilon = p_0 [-(1 - R) \log(1 - \varepsilon - R)]_0^\varepsilon \quad (44)$$

Combining equation (43) and (44) leads to equation (45).

$$\frac{W_g}{\sigma_g} = - \frac{(1 - \varepsilon - R)(1 - R) \log(1 - \varepsilon - R)}{\varepsilon} - \frac{\varepsilon(1 - \varepsilon - R)}{\varepsilon} + \frac{(1 - \varepsilon - R)(1 - R) \log(1 - R)}{\varepsilon} \quad (45)$$

To find the shoulder point, which is the optimal ratio $\frac{W_g}{\sigma_g}$, the derivative with respect to the strain must be zero. Substitute $R = 1 - P$, as can be seen in equation (46).

$$\frac{d}{d\varepsilon} \left(\frac{W_g}{\sigma_g} \right) = \frac{P^2 \log(P - \varepsilon) + P^2 (-\log(P)) + \varepsilon(P + \varepsilon)}{\varepsilon^2} = 0 \quad (46)$$

In case of 100% porosity, then $P = 1$, previous equation can be simplified to equation (47).

$$\log(1 - \varepsilon) + \varepsilon^2 + \varepsilon = 0 \quad (47)$$

This expression has two solutions, namely $\varepsilon = 0 \vee 0.6838$, where the first solution is a trivial solution. That turns out that the $\varepsilon_{\text{at } \frac{W_g}{\sigma_g} \text{ max}} = 0.6838$.

Appendix C – Codes

This appendix discusses the codes used in ARDUINO and PROCESSING 2.2.1 and is complement to section 3.2.2 of the main report.

In ARDUINO the next code is used. The analog port to read is in this specific case A4, but more interesting is the delay in microseconds. Because there is no delay ARDUINO reads data at a sample frequency of 32 kHz, which is the maximum sample frequency of the analog port. The baud rate is set to 115200 and has to be filled in as shown.

```
int port = A4;    // Analog Port to read
int wait = 0;    // Delay in microseconds

void setup() {
  Serial.begin(115200);
}

void loop() {
  Serial.print(millis());
  Serial.print("\t");
  Serial.println(analogRead(port));
  delayMicroseconds(wait);
}
```

In PROCESSING 2.2.1 the next code is used to process the data into a text file. It reads the data and transform it into a string. As shown, the baud rate is of importance here as well. The data is stored in a text file and a name can be given to this file.

```
import processing.serial.*;

Serial mySerial;
PrintWriter output;
void setup() {
  mySerial = new Serial(this, Serial.list()[0], 115200);
  output = createWriter("Name.txt"); // Give name of output
}

void draw() {
  if (mySerial.available() > 0 ) {
    String value = mySerial.readString();
    if ( value != null ) {
      output.println( value );
    }
  }
}

void keyPressed() {
  output.flush(); // Writes the remaining data to the file
  output.close(); // Finishes the file
  exit(); // Stops the program
}
```